Uncovering the Structure of the Galactic Bulge Using Kinematic Data from the JASMINE Near-Infrared Astrometric Satellite

by

Jitrapon Lertprasertpong

Submitted to the Department of Physics
in partial fulfillment of the requirements for the degree of

Bachelor of Science in Physics

at the

MASSACHUSETTS INSTITUTE OF TECHNOLOGY

June 2021

Author .....
Department of Physics
May 14, 2021

Certified by .....
Stephen Levine
Astronomer & LDT Scientist, Lowell Observatory
Thesis Supervisor

Certified by .....
Mark Vogelsberger
Associate Professor of Physics
Thesis Supervisor

Accepted by .....
Deepto Chakrabarty
Associate Head of Physics, Department of Physics

Uncovering the Structure of the Galactic Bulge Using Kinematic Data from the JASMINE Near-Infrared Astrometric Satellite

by

Jitrapon Lertprasertpong

Submitted to the Department of Physics
on May 14, 2021, in partial fulfillment of the
requirements for the degree of
Bachelor of Science in Physics

Abstract

The Galactic Center (GC) is the region with the most extreme stellar densities, a strong gravitational field, and the most prolific star formation region in the Milky Way. Furthermore, the Milky Way is the only galaxy that we can resolve individual structure such as Nuclear Stellar Disk (NSD) and Nuclear Bulge (NB) from the whole bulge structure. These reasons make the observation of the Galactic Center appealing to astronomers. Due to the high extinction from interstellar dust in the visible band ($A_V \approx 30$ mag), it is necessary to study the Galactic Bulge in the Near-Infrared (NIR) band. JASMINE mission is designed to observe the Galactic Nuclear Bulge at the region of 100-300 parsecs from the Galactic Center in the Near-Infrared band. In this thesis, we evaluate the capability of the JASMINE satellite in studying the galactic bulge structure in several aspects, including the JASMINE's capability to distinguish gravitational potential models at the Galactic Bulge, possible uncertainties in JASMINE parallax and proper motion measurements, and the population of stars that JASMINE can observe. The result of this study indicates that JASMINE can distinguish two limiting cases of mass distribution: point mass, and homogeneous sphere within the proper motion accuracy in the order of 10 mas/year. In addition, we also notice that the accuracy of 25 μas for parallax measurement would result in the probability of 45% to mistake bulge star as disk stars. Finally, we also conclude that the sample population of stars suitable for JASMINE are Giants with a sample size of approximately 2.6×10^5 stars.

Thesis Supervisor: Dr. Stephen Levine
Title: Astronomer & LDT Scientist, Lowell Observatory

Thesis Supervisor: Professor Mark Vogelsberger
Title: Associate Professor of Physics

Acknowledgments

From the accomplishment of this study, the author would like to thank Dr. Stephen Levine for providing me invaluable supports in the simulation techniques of the physics of Galactic Bulge and proofreading of this thesis. From our weekly meeting, I gradually learn various insights into galactic astronomy research and the method to search for scientific literature. I also would like to thank Prof. Mark Vogelsberger for teaching me the basics of galactic astronomy and check the accuracy of my thesis. The knowledge in galactic and extragalactic astronomy from his astrophysics class is incredibly helpful in studying the kinematics of the Galactic Bulge.

Furthermore, I would like to thank the MIT community and physics department for supporting me throughout my undergraduate years. The environment at this place challenges me to keep seeking scientific knowledge far beyond my imagination. The scientific knowledge I learned here helps me understand and appreciate the beauty of the universe more. Furthermore, humanity courses at MIT also help me grow as a person and connect with many people worldwide, inside and outside the scientific community.

In addition, I would like to thank my family and my friends for their constructive supports and helpful advice. Especially during the difficult time of the COVID-19 pandemic, the preparation of this thesis has become more challenging. The emotional supports from my family and my friends help me get through this difficult time properly. I cannot say thank you enough for everyone's support for the accomplishment of this thesis.

Contents

List of Figures

List of Tables

Chapter 1

Introduction

1.1 Structure of the Milky Way

The Milky Way galaxy is believed to be a barred spiral galaxy within the SBc category of the Hubble classification. It is also the second-largest galaxy in the Local Group, a group of galaxies consisting of three large and over 30 smaller galaxies [23]. Milky Way is the most well-known galaxy to humans for an apparent reason: we live in it. However, living inside the Milky Way disk brings about difficulties in studying the large-scale structure of the Milky Way directly from the inside.

The early attempt in studying the structure of the Milky Way started from the mapping of stars positions by William Herschel [13]. His method of using a telescope to count the stars in numerous sky patches helped him create the early map of the Milky Way shown in Fig.1-1.

From our current knowledge, the map is inaccurate since Herschel assumed that stars are distributed uniformly, and the number of stars is related only to the distance to the Milky Way boundary, which we know that it is not true [28]. In the present day, apart from new techniques to study the structure of the Milky Way, such as the studies of stellar orbits and neutral hydrogen emission, star-counting is still a standard method to study the Milky Way structure. Nevertheless, star-counting still has various challenges, such as the stellar crowding of the field and large interstellar extinction, especially in the central part of the Milky Way. To reduce these

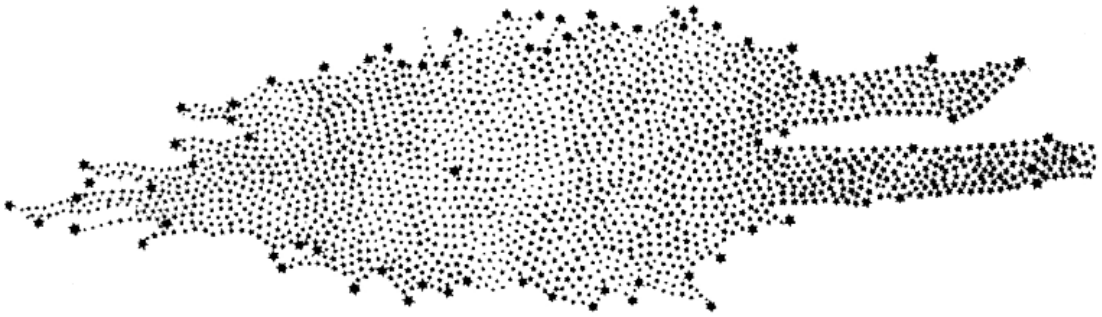

Figure 1-1: The map of the Milky Way created by the star-counting method by William Herschel [13]. The map is created using the assumption that stars are distributed uniformly with the sun at the center indicated by a large star symbol.

effects, observation in the near-infrared (NIR) spectrum is necessary. With present-day knowledge, astronomers now divide the main components of the Milky Way into the central supermassive black hole, Galactic Bulge, Bar structure, galactic disk, and halo.

1.1.1 Central Supermassive Black hole

The central part of the Milky Way is a strong radio source called Sagittarius A* (Sgr A*). Various studies of stellar orbits around Sgr A* reveals that Sgr A* is a compact mass of $(4.154 \pm 0.014) \times 10^6\ M_\odot$ [2], implying the existence of supermassive black hole [10]. Supermassive black holes always present in the bulge structure and stellar spheroid of both elliptical and disk galaxies [19].

1.1.2 Galactic Bulge

The Galactic Bulge (GB) is the highly-dense region at the center of the Milky Way. In this study, we use the definition of the boundary of the Galactic Bulge as the region with the radius of less than two kpc from the Galactic Center [34]. The innermost structure of the Galactic Bulge is the Nuclear Stellar Cluster (NSC) enclosing Sgr A*. This structure is a massive structure composed of old and complex stellar population [26]. The nuclear stellar cluster also resides in a larger structure called

the Nuclear Bulge (NB), which is a dense, massive, disk-like structure with radius of approximately 230 pc and scale height of about 45 pc [17]. The Milky Way galaxy is the only galaxy that we can resolve nuclear stellar cluster and nuclear bulge directly. Thus, the Galactic Bulge region is the main target for astronomers to understand the central structure of barred spiral galaxies.

1.1.3 Bar Structure

Bar structure is the structure that appears in various galaxies. The structure can be observed by star counting and the brightness distribution of stars. Furthermore, the dynamics of the bar can be studied from the study of gas flow using H I and CO spectra. From the data from COBE, the orientation of the bar structure can be approximated as $15^\circ \lesssim \varphi_{bar} \lesssim 35^\circ$, where φ_{bar} is the angle measured between the major axis of the bar and the line from the sun to the Galactic center in the $l > 0$ direction [9].

1.1.4 Galactic Disk

The galactic disk is the axisymmetric region containing the majority of stars in the Milky Way [4]. The disk of a spiral galaxy can be divided into a thin disk with thickness about 1,000 light years above and below the galactic plane and a thick disk ranging 3,500 light years above and below the galactic plane. The total diameter of the Milky Way disk is considered to be approximately 120,000 light years, where the sun is at about 28,000 light years or about 8 kpc from the Galactic Center [6].

1.1.5 Galactic Halo

The galactic halo can be considered as the least known region of the Milky Way. The halo can be divided into the stellar halo, which contains metal-poor globular clusters contributing about 1% of the stellar mass of the galaxy, and dark halo, which contains mostly dark matter [4]. The halo is a structure that is generally too dim to observe

using telescopes. Nevertheless, it exerts a strong gravitational influence on the galaxy from dark matter.

1.2 Observation of the Galactic Center

The Galactic Center (GC) is the region with the most extreme stellar density and most prolific star formation rate in the Milky Way [26]. With unique structures such as the supermassive black hole, nuclear bulge (NB), and nuclear stellar disk (NSD), which is clearly separated from the Galactic Bulge, this region provides a myriad of possibilities to study the formation and evolution of the Galactic Center.

In this thesis, we adopt the distance between the solar system and Galactic Center from Abuter et al. (2019), measured to be approximately 8.2 kpc [2]. With this distance, mapping the positions and velocities of stars require extremely high precision at about < 100 micro-arcseconds (μas). After the launch of the Gaia satellite in 2013, it is possible to map the structure of the Milky Way precisely in a visible band. The data release from Gaia provided various new information about both the disk and the halo. However, the region around several hundred parsecs from the Galactic Center is still challenging to study using optical telescopes due to the large interstellar extinction of $A_V \approx 30\ mag$. The more suitable electromagnetic spectrum for studying the Galactic Center would be the near-infrared (NIR) spectrum, which has the extinction coefficient of $A_k \approx 2.5\ mag$ [25].

JASMINE (Japan Astrometry Satellite for Infrared Exploration) is the astrometric mission executed by JAXA (Japan Aerospace Exploration Agency) to study the Galactic Nuclear Bulge in the Near-Infrared spectrum. Since JASMINE mission is claimed to have the precision at the same level as Gaia, but in the Near-Infrared band, JASMINE provides promising capabilities to explore the structure of the Galactic nuclear bulge in the region that is unresolved by other telescopes. By resolving the Galactic nuclear bulge structure, we expect to have a new understanding of the structure, formation, and evolution of the Galactic Center.

1.3 Astrometric Measurement

Since the primary technique to study the Galactic Bulge is performed through astrometric measurement, it is crucial to start by reviewing the concept of astrometric measurement. Astrometry is the technique of the measurement of the stellar positions at specific times. Sufficient data in stellar positions at different times can help astronomers determine the velocity and possibly even acceleration of celestial objects. The precise measurement of the positions and velocities of stars plays an essential role in the understanding of kinematics and dynamics of all celestial objects, including planets, stars, galaxies, and satellites. Furthermore, precise measurement of positions and velocities of celestial objects will help us create a reference frame for all celestial objects.

Astrometry has a long history centered around the making of the star catalog. Starting from around 190 BC, Hipparchus of Nicaea started recording the position of over 850 stars and made it into the first extensive star catalog. He also formed the basis of the stellar magnitude scale we use in the present day [20].

After a long development of angle measurement throughout human history, the measurement of stellar parallaxes and proper motions becomes possible when the precision of angle measurement reaches the scale of about arcseconds. Proper motion of stars was measured for the first time in 1718 by Edmond Halley [5]. In 1807, Friedrich Bessel successfully measured parallaxes of 61 Cygni with the parallax angle of 0.3 arcseconds [15]. The discovery of proper motions and parallaxes indicated that stars are no longer independent luminous objects but rather objects with their positions and velocities.

The astrometric measurement depends heavily on the photographic plates and photodetectors. With the invention of charge-coupled devices (CCDs) in the 1980s, the uncertainties in astrometric measurement was reduced to 1 milli-arcseconds (mas) or better [22]. CCDs also reduced the cost of image detector significantly, resulting in an easier access of astrometry to amateur astronomers.

Another revolution of astrometry started when space telescope was launched. In

1989 when European Space Agency sent Hipparcos satellite into orbit. With Hipparcos satellite, the Hipparcos catalog of 118,218 stars was created [1]. Even though the parallax and proper motion measurement of individual star of Hubble Space Telescope and ground based telescopes could rival those of Hipparcos, Hipparcos had the advantage of having larger sample to unprecedented accuracy for the sample size. Thus, Hipparcos star catalog became the most precise measurement of parallaxes and proper motion of stars than ever before at that time.

In 2013, the Gaia satellite was launched into orbit. With Gaia satellite, over billion of stars in the Milky Way was mapped. Astronomers are able to map the structure of the Milky Way with great precision for the first time. However, Gaia has the limitation when observing in the crowding field and extinction along the Galactic plane and Galactic Center. Therefore, the astrometric measurement in Near Infrared (NIR) band is necessary. JASMINE will play an important role in mapping stars in the galactic bulge to fulfill the data from Gaia mission.

JASMINE (former name: Small-JASMINE) mission will perform the astrometric measurement of stars by measuring both parallaxes and proper motions. From these measurements, we will be able to create 5-dimensional phase space distribution of stars in the Galactic Nuclear bulge to study the formation and evolution of the Galactic Bulge structure.

The precise astrometric measurement of the galactic bulge is crucial to modern astronomy research. Firstly, we can get the information about the gravitational field of the Galactic Bulge using the measurement of positions and velocities of stars. Besides, the data taken by JASMINE will reveal the structure of the Galactic nuclear bulge that astronomers have never observed before due to the crowding and extinction in optical band. Moreover, JASMINE data will expand the data from the region that is obscured to Gaia. The catalog of Gaia and JASMINE will help astronomers map the Milky Way with higher precision than ever.

Chapter 2

Galactic Bulge Kinematics

In this chapter, we evaluate JASMINE's ability to clarify the nuclear bulge structure by simulating various mass distribution models of the Galactic Bulge. Then, we study how much precision JASMINE needs to distinguish two extreme cases of mass distribution: point mass distribution, and homogeneous sphere. We also study the JASMINE's capability to distinguish between two different structural supports of the nuclear bulge including pure rotational support and pure pressure support. In addition, we also study the effect of additional pattern speed of the bulge on the kinematics of the nuclear bulge.

2.1 Stellar and Gas Kinematics near Galactic Center

The Galactic Bulge is the dense central region of the Milky Way which consists mainly of old and evolved stars. In this region, we are interested in many properties such as gravitational potential and mass density distribution. The kinematics of the Galactic Bulge can be studied based on positions and velocities of stars and gas in the Galactic Bulge. Since the stellar component can be described as collisionless, we can write the equation of motion for dynamical tracers as follows [19]

$$n\frac{\partial \Phi}{\partial r} = \frac{\partial (n\sigma^2)}{\partial r} + \frac{n}{r}\bar{v_\phi}^2 \tag{2.1}$$

Eq. 2.1 is the Jeans equation along the equatorial plane of a cylindrically symmetric system where n is the number density of stars, $\bar{v_\phi}$ is the mean velocity of stars, σ is the one dimensional velocity dispersion, and Φ is the gravitational potential of the system. For spherical system, we can further simplify Eq. 2.1 into

$$GM_{\text{enclosed}} = r(\sigma^2 + \bar{v_\phi}^2) + r\sigma^2 \left[-(\frac{\partial \log(n)}{\partial \log(r)} + 1) - \frac{\partial \log(\sigma^2)}{\partial \log(r)} \right] \tag{2.2}$$

where M_{enclosed} is the interior mass enclosed within radius r. From Eq. 2.2, the terms inside brackets can be neglected since the Galactic Center has $n \sim r^{-1}$ and σ varying slowly with radius [19]. Since Eq.2.2 shows that we have the square combination of bulge motion and random motion. Therefore, it is useful to combine two terms together into root-mean-square velocity ${v_{rms}}^2 = \sigma^2 + \bar{v_\phi}^2$ which corresponds to the virial equilibrium of the system. We can write the velocity of stars around the Galactic Center as

$${v_{rms}}^2 = (\sigma^2 + \bar{v_\phi})^2 = \frac{GM_{enclosed}}{r} \tag{2.3}$$

In this thesis, we create a simple dynamical model of the Galactic Bulge to study the capability of JASMINE to distinguish between different dynamical models. Since the main focus of JASMINE is the Galactic nuclear bulge with the radius of 100-300 pc from the Galactic Center, the dynamical effect of large-scale structure of the Milky Way such as the galactic bar, galactic disk, and the influence from dark matter can be considered negligible. This claim can be confirmed using the information that the size of the galactic long bar which is approximately 5 kpc from the Galactic Center [28]. Since the enclosed mass becomes smaller for extended objects, we expect that the gravitational influence is negligible in smaller scale. Furthermore, the effect of dark matter is negligible since the dark matter contribution to the kinematics of stars and gas increases as a function of galactocentric radius [29]. Therefore, at small distance from the Galactic Center, this effect is negligible.

2.2 Mass Distribution of the Galactic Bulge

Since the galaxy is a highly complex dynamical system, to describe the kinematics of stars and gas in the galaxy, we start from describing the galaxy as a smooth collective potential well. According to Poisson's equation, the mass distribution is the source of gravitational potential well, which results in the overall kinematics of the system. The relation between mass density and potential of the system can be described as

$$\nabla^2\Phi = 4\pi G\rho \tag{2.4}$$

We can also write Eq.2.4 as the form of mass density ρ

$$\rho = \frac{\nabla^2\Phi}{4\pi G} \tag{2.5}$$

Using the assumption we previously mentioned, stellar support against gravity is provided by a combination of systematic or bulk motion and random motion equivalent to pressure support. The stars in nearly circular orbits have the speed defined by circular velocity $v_c(r)$ which is related to the potential Φ of the system as

$${v_c}^2 = \vec{r} \cdot \nabla\Phi \tag{2.6}$$

Since Galactic Bulge can be approximated as a spherical system, we can further simplify Eq.2.6 to have the same form as Eq.2.3

$${v_c}^2 = \frac{GM_{enclosed}(r)}{r} \tag{2.7}$$

Eq.2.7 implies that if we can determine v_c as a function of r, we can estimate $M(r)$ using Eq.2.7. By approaching from the mass distribution, we can create a simple model of the galactic kinematics. Since the velocity distribution of stars varies by the mass distribution, we can evaluate the precision JASMINE need to distinguish between each mass distribution models.

In this study, we will focus on three mass distributions according to the complexity.

Starting from two limiting cases: point-mass potential, and uniform mass distribution. Then, we will compare two limiting cases to a more realistic Galactic Bulge model which is the Plummer model.

2.2.1 Point-mass Distribution

Point mass distribution serves as a limiting case where all the mass of the Galactic Bulge is concentrated at the center of the Galactic Bulge. It is clear that this model is nonphysical according to the observational data. However, we can use this model as the constraint of the kinematics of the Galactic Bulge. The point-mass potential derived from this mass distribution is given by

$$\Phi(r) = -\frac{GM}{r} \tag{2.8}$$

where M is the total mass of the system.

2.2.2 Homogeneous Sphere Model

Another limiting case of mass distribution is to assume that the mass density ρ of the bulge is constant throughout the bulge. Due to the nature of linear rotation curve near the Galactic Center, this model serves as a good approximation for the Galactic Bulge.

For the homogeneous sphere with outer radius of the homogeneous sphere a and constant density ρ, the gravitational potential, derived from Poisson equation, is given by

$$\Phi(r) = \begin{cases} -2\pi G\rho(a^2 - \frac{1}{3}r^2) & r \leq a \\ -\frac{4\pi G\rho a^3}{3r} & r > a \end{cases} \tag{2.9}$$

2.2.3 Plummer Model

Plummer model describes the mass distribution of spherical systems such as globular clusters. This model was first used by H.C. Plummer to fit the density profile of

globular clusters [27]. The potential for this mass distribution is given by

$$\Phi(r) = -\frac{GM}{\sqrt{r^2 + b^2}} \tag{2.10}$$

where b is the Plummer scale length. This potential fixes the problem of having singularity at the center of the system unlike the point mass potential.

2.2.4 Miyamoto-Nagai Model

Miyamoto-Nagai model is the modification of Plummer potential that can describe various component of a galaxy from the disk-like structure to a sphere [21]. This density model is a cylindrically symmetric model in which we can describe its potential as

$$\Phi(r) = -\frac{GM}{\sqrt{R^2 + (a + \sqrt{z^2 + b^2})^2}} \tag{2.11}$$

If we consider the potential along the galactic plane or the case where $a = 0$, Miyamoto-Nagai potential can be reduced to Plummer potential. Since Miyamoto-Nagai potential has the ability to model both spherical and cylindrical components, we can create a more realistic models of the bulge, disk, and halo components using the combination of several Miyamoto-Nagai potentials.

In this study, the models that we are going to use for describing the Galactic Bulge models are point mass model, homogeneous sphere model, and Plummer model. Miyamoto-Nagai model will be used to describe the gravitational influence from the Galactic Disk.

2.3 Modeling the Mass Density

Starting from different mass distributions, we can get different kinematics of the system. By using Poisson's equation, mass density of the Galactic Bulge can be described using Eq.2.5. Then, we can describe the form of mass density in each model as in Table 2.1.

Table 2.1: The summary of gravitational potential models and their mass density

Models	Density
Point mass	$\rho(r) = M\delta(r)$
Homogeneous Sphere $(r < a)$	$\rho(r) = \dfrac{3M}{4\pi a^3}$
Homogeneous Sphere $(r > a)$	$\rho(r) = 0$
Plummer model	$\rho(r) = \dfrac{3M}{4\pi b^3}\left(1 + \dfrac{r^2}{b^2}\right)^{-5/2}$
Miyamoto-Nagai model	$\rho(R,z) = \frac{b^2M}{4\pi}\frac{aR^2+(a+3\sqrt{z^2+b^2})(a+\sqrt{z^2+b^2})^2}{[R^2+(a+\sqrt{z^2+b^2})^2]^{5/2}(z^2+b^2)^{3/2}}$

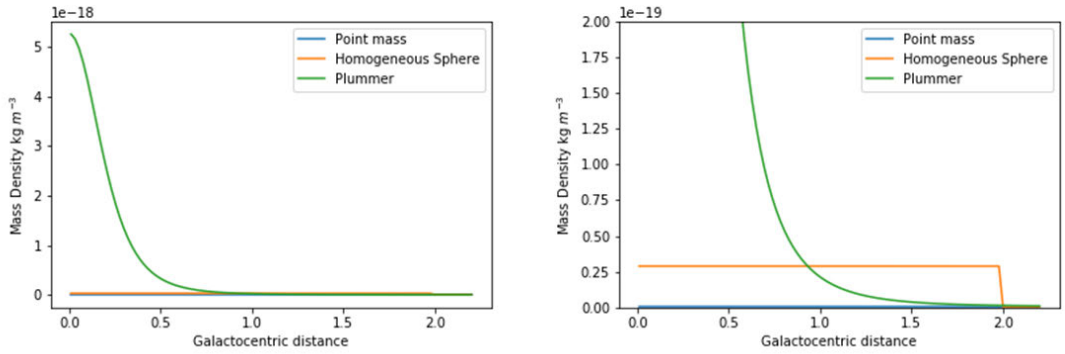

Figure 2-1: Mass density distribution of different gravitational potentials. The plot on the left is the total mass density distribution of three different models. The plot on the right is the re-scaled plot to signify the difference between homogeneous sphere model and point mass model.

Using the result in Table 2.1, we can find the rough estimate of mass distribution of the Galactic Bulge as shown in Fig.2-1.

2.4 Milky Way Velocity Curves

The structure of the galaxy is supported by the combination of systemic or bulk motion and random motion. As discussed above, we can describe the kinematics of stars in the Galactic nuclear bulge using Eq.2.3 where v_ϕ is the mean streaming velocity of stars representing bulk motion about the galaxy center and σ is the velocity dispersion representing pressure support. Furthermore, Eq.2.3 also implies that the

Table 2.2: The summary of mass distribution models and their velocities

Mass distribution models	Root-mean-square velocity
Point mass	$v_{rms}(r) = \sqrt{\frac{GM}{r}}$
Homogeneous Sphere ($r < a$)	$v_{rms}(r) = \sqrt{\frac{4}{3}\pi G\rho r}$
Homogeneous Sphere ($r > a$)	$v_{rms}(r) = \sqrt{\frac{4\pi G\rho a^3}{3r}}$
Plummer model	$v_{rms}(r) = \sqrt{GM\frac{r^2}{(r^2+b^2)^{3/2}}}$
Miyamoto-Nagai model	$v_{rms}(r) = \sqrt{\frac{GM}{(R^2+(a+\sqrt{z^2+b^2}))^3}\eta(R,z)}$ where $\eta(R,z) = R^2 + z^2(\frac{a+\sqrt{z^2+b^2}}{\sqrt{z^2+b^2}})$

total root-mean-square velocity of stars as a function of galactocentric radius is conserved. Using this information, we can find the kinematic signature of different mass distribution as shown in Table 2.2.

From the information we have, we can visualize the kinematics of different models as shown in Fig.2-2.

2.5 Modeling the Galactic Disk and Galactic Halo

Although this thesis focuses on the effects of Galactic Bulge potentials on the kinematics of stars, other parts of the Milky Way, such as the supermassive black hole, galactic disk, and galactic halo also play a substantial part in the kinematics of stars. To study the dynamic of stars in the bulge due to gravitational potentials, we will fix the gravitational potentials of other parts of the Milky Way and vary the models of the gravitational potentials of the bulge. In this study, we use the model from Dauphole & Colin (1995) [7] to model the kinematics of stars under different Galactic Bulge models. The main advantage of Dauphole & Colin is that the overall gravitational potentials are the summation of all gravitational potential from different parts of the Milky Way as shown in Eq.2.12. Using this method, we can make an analytic

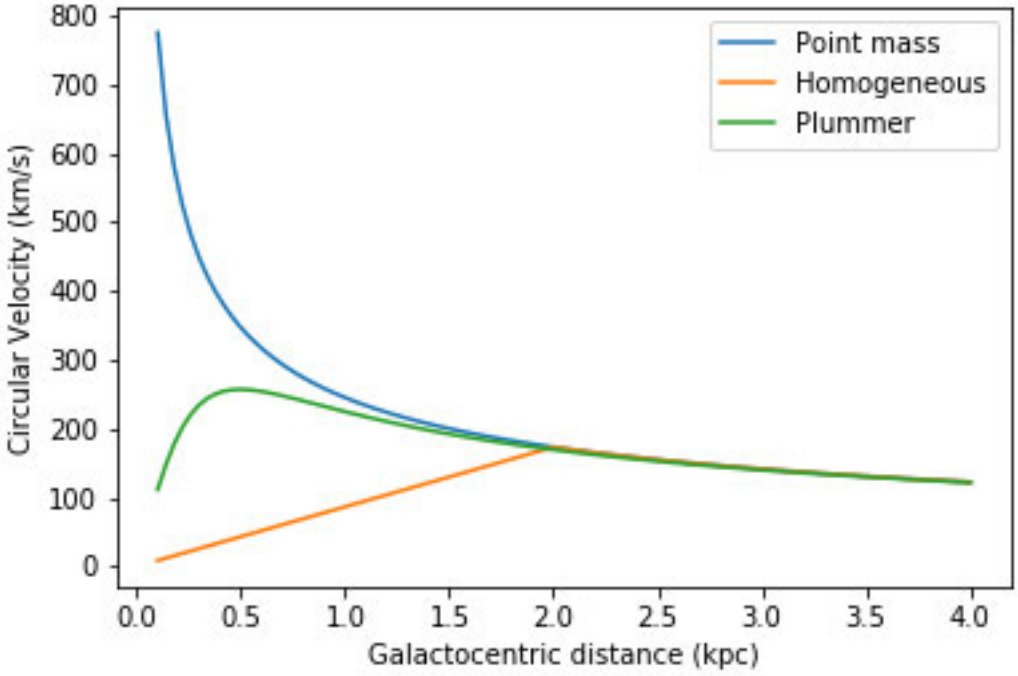

Figure 2-2: Velocity Curves of stars in the Milky Way considering effect from the different mass distribution models of the Galactic Bulge only.

Table 2.3: The parameters of different parts of the Milky Way taken from Dauphole & Colin [7]

Components	Parameters
Disc	$M_d = 7.9080 \times 10^{10} M_\odot$ $a_d = 3.55$ kpc $b_d = 0.25$ kpc
Halo	$M_h = 6.9776 \times 10^{11} M_\odot$ $b_h = 24.0$ kpc
SBH	$M_{SBH} = 4.154 \times 10^6\ M_\odot$
Bulge	$M_b = 1.3955 \times 10^{10}\ M_\odot$

model of each part of the galaxy separately, which is quick to compute.

$$\Phi_{total} = \Phi_{bulge} + \Phi_{BH} + \Phi_{Disk} + \Phi_{Halo} \tag{2.12}$$

The parameters of the components of each Milky Way is derived from Dauphole & Colin is shown in the Table 2.3.

Using this model, we can easily compare the kinematics of each models by varying the gravitational potential of the Galactic Bulge only without affecting the gravitational potential of other parts of the Milky Way. In Dauphole & Colin model, the Galactic Disc is modeled using Miyamoto-Nagai model [7]. The Galactic Halo is modeled using the Plummer model, which is a limiting case of the Miyamoto-Nagai potential. The parameters for the gravitational potentials of the Milky Way are given in Table 2.3.

By varying the gravitational potentials from the Galactic Bulge and fixing the potentials from other components of the Milky Way, we can visualize the influence of gravitational potential models on the velocity of stars as shown in Fig. 2-3.

2.6 Proper Motion of Stars

Since the solar system is located at about 8.2 kpc from the center of the Milky Way [2], the kinematics of stars in the Milky Way can be studied through the proper

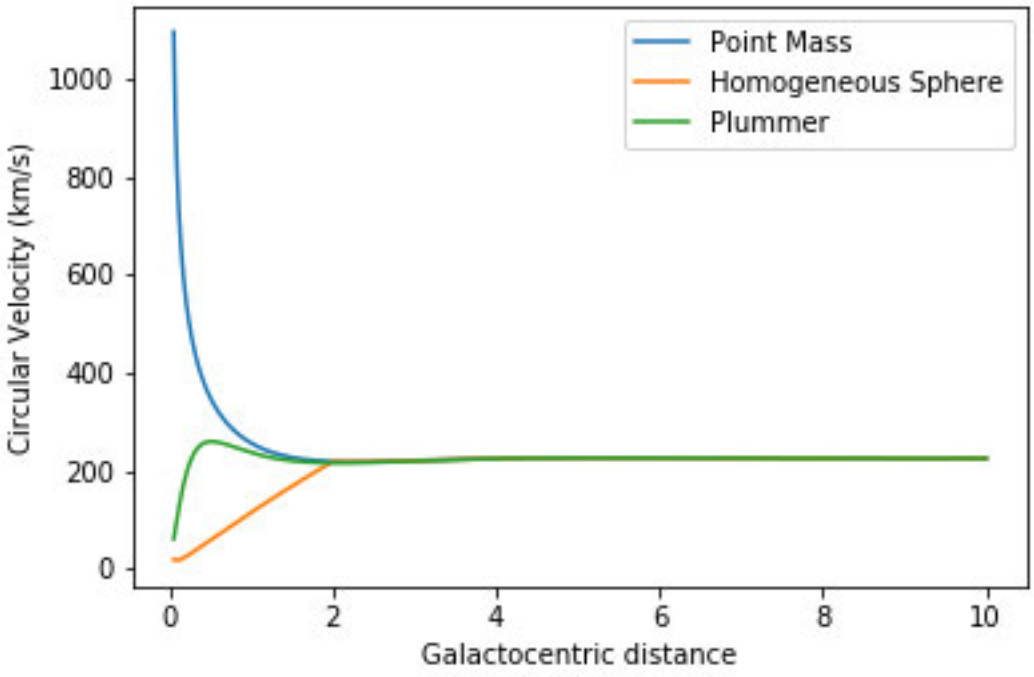

Figure 2-3: Velocity Curves of the Milky Way as a function of Galactocentric distance

motion of stars. Proper motion of stars along with position of stars from JASMINE give the information about 5-dimensional phase space of stars under the gravitational potential Φ of the system. Now, since proper motion measured by JASMINE consists of galactic latitudinal proper motion μ_b and galactic longitudinal proper motion μ_l. While both proper motions can describe the kinematics of stars in the Galactic nuclear bulge, we choose to use galactic longitudinal proper motion μ_l to describe the proper motion of stars in this thesis since generally the intrinsic angular momentum of the Galactic Bulge creates the rotation along the Galactic plane. Therefore, describing proper motion along the galactic plane is a suitable choice in this case.

Since Proper motion is the apparent tangential motion of stars observed from the solar system, we need to consider the effect of both stars and local velocity of the solar system relative to the Galactic Center. We define an inertial frame of reference traveling along the Galactic Rotation and centered around the sun as the Local Standatard of Rest (LSR). In this thesis, we will use LSR frame as a

reference frame of motion. The velocity of LSR relative to the Galactic Center is $v_{LSR} = 220 \pm 20$ km/s [4]. Note that the sun has its own velocity relative to LSR of 13.4 km/s [4] pointing in the direction of $l = 28°$ and $b = 32°$ and there is also the combination of the Earth's motion and JASMINE's orbit around the sun. However, for simplicity, we approximate the proper motion distribution of stars as the order of magnitude approximation. Therefore, we will use LSR frame in this study. The description of the orbit is shown in the Fig.2-4.

From the orbit described above, we can write the proper motion in the unit of milli-arcseconds year^{-1} (mas/yr) as follows

$$\mu(mas/yr) = \frac{0.2109 \cdot v_{\perp}(km/s)}{s(kpc)} \tag{2.13}$$

where s is the distance between the sun and observed stars and $v_{\perp}$ is the vector subtraction between velocity of stars and LSR projected on the plane of the sky.

To model the proper motion distribution, we can simulate two types of limiting cases: pure bulk rotation, and purely random pressure.

2.6.1 Pure Bulk Rotation

In the case where the motion of stars in the Galactic Bulge is purely bulk motion, we will have $v_{rms} = v_{\phi}$ and velocity dispersion $\sigma = 0$. In this case, we assume that all stars rotate in the clockwise direction with velocity v_{ϕ}. In this case, the perpendicular velocity $v_{\perp}$ in Eq.2.13 can be written explicitly as $v_{\perp} = v_{\phi} - v_{LSR}$, where v_{LSR} is the velocity of LSR relative to the Galactic Center. From this relation, the difference in proper motion distribution comes directly from the effect of mass distribution on v_{ϕ}. Furthermore, since we consider the proper motion purely from bulk motion, in this case, the proper motion distribution will be narrow for each model as shown in Fig.2-5.

From Fig.2-5, we can see that the difference between proper motion value in between the limiting case of point mass model and homogeneous sphere has the value of over 10 mas/year.

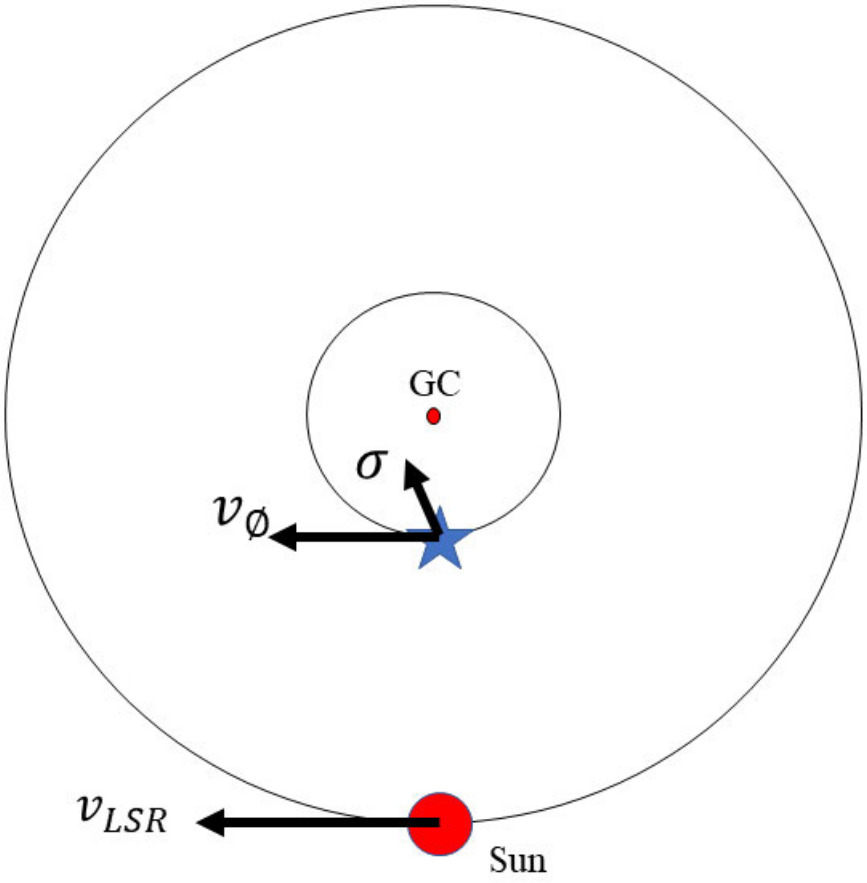

Figure 2-4: Schematic of the orbit of stars near the Galactic Center. The velocity is the combination of systematic motion v_{phi} and random velocity dispersion σ.

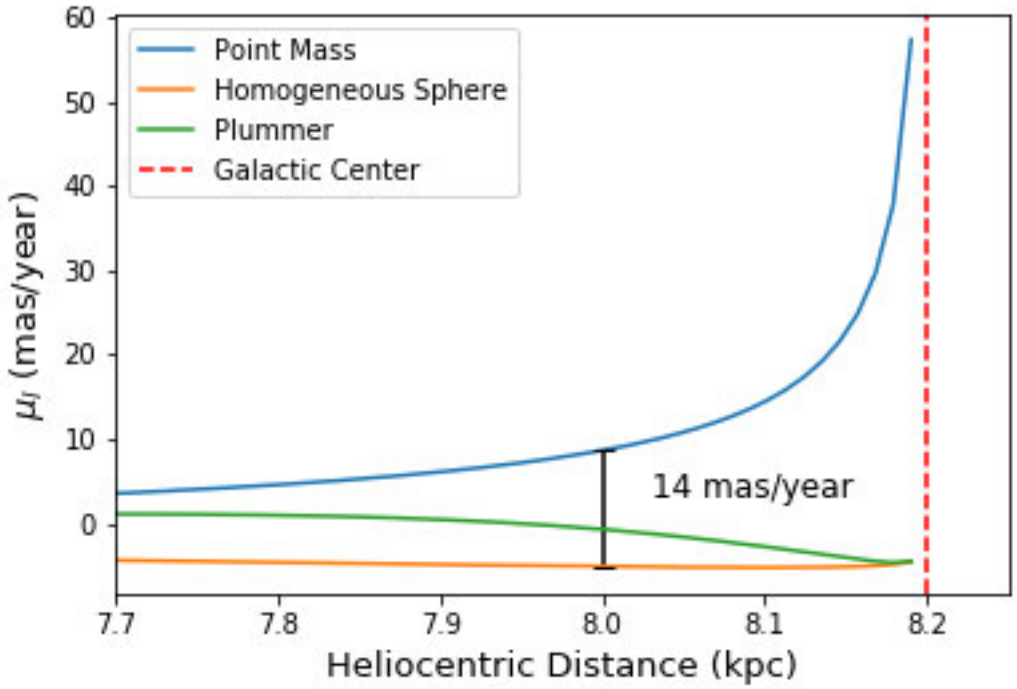

Figure 2-5: Proper motion distribution along the galactic plane for pure bulk motion. In this case, the distribution of proper motion is narrow for each model since all stars travel in the same direction. The discrepancy between homogeneous sphere and point mass potential is at about 14 mas/year at 200 pc from the Galactic Center.

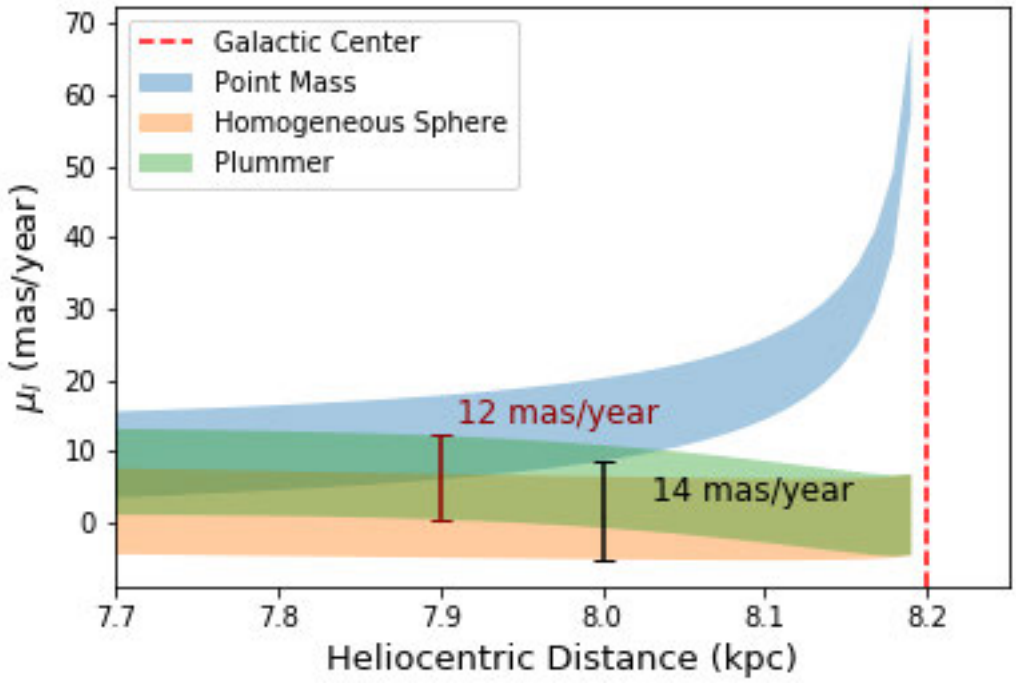

Figure 2-6: Proper motion distribution along the galactic plane for pure pressure support. In this case, the proper motion distribution is broadened due to the random motion of stars. The discrepancy between model is still at 14 mas/year 200 pc from the Galactic Center. Nevertheless, the random motion broadens the proper motion distribution making the difference between maximum and minimum proper motion to be approximately 12 mas/year for Plummer model at 300 pc from the Galactic Center

2.6.2 Pure Pressure Support

Another limiting case we can consider is the case of pure pressure support. In this case, we set $v_{rms} = \sigma$ and systematic motion $v_\phi = 0$. In this case, we assume that stars have velocity of σ in random direction. Thus, the proper motions along the galactic plane are calculated using the projection of $\vec{\sigma} - \vec{v}_{LSR}$ onto the galactic plane, perpendicular to the observer. Therefore, the distribution of proper motion will spread out into the range of upper and lower limit of proper motion. The plot of proper motion distribution is shown in Fig.2-6

From Fig.2-6, at the distance of approximately 200 pc from the Galactic Center, we observe the difference between each proper motion distribution as approximately

14 mas/year. Besides, the broadening of proper motion distribution has the value of approximately 12 mas/year.

Comparing between pure bulk motion and pure random motion, to distinguish between different mass distribution models and different gravitational support of the nuclear bulge, JASMINE needs to have proper motion precision better than the order of magnitude of 10 mas/year. As we will discuss in chapter 3 and 4 of this thesis, the proper motion precision of JASMINE is approximately 125 μas/year or 0.125 mas/year for faint stars in the Galactic Bulge [34]. Thus, JASMINE is a suitable mission for this task.

2.7 Rotating Bulge

Since the Galactic Bulge also contains intrinsic angular momentum, it is expected that Galactic Bulge rotates around the Galactic Center with a certain pattern speed. From the direct determination of the pattern speed of the bar and the hydrodynamic models, the pattern speed of the Galactic Bulge can be approximated to be in the range of $\Omega_b = 50 - 60\ km\ s^{-1}\ kpc^{-1}$ [8].

The pattern speed of the Galactic Bulge creates the coriolis force which adds additional velocity components into the system.

$$\vec{v}_{total} = \vec{v}_{rms} + \vec{\Omega_b} \times \vec{r} \tag{2.14}$$

Eq.2.14 implies that the result from pattern speed will become prominent at higher galactocentric distance r. The result shown in Fig.2-7 indicates that the effect of pattern speed will be more significant at higher galactocentric distance. At distance around 200 pc from the Galactic Center, we can see that the difference between proper motion distributions are approximately 0.3 mas/year. Hence, JASMINE needs to have proper motion precision better than 0.3 mas/year in order to detect the effect from the additional rotation of the bulge. From JASMINE proper motion precision of 0.125 mas/year, we expect that JASMINE should be able to distinguish between

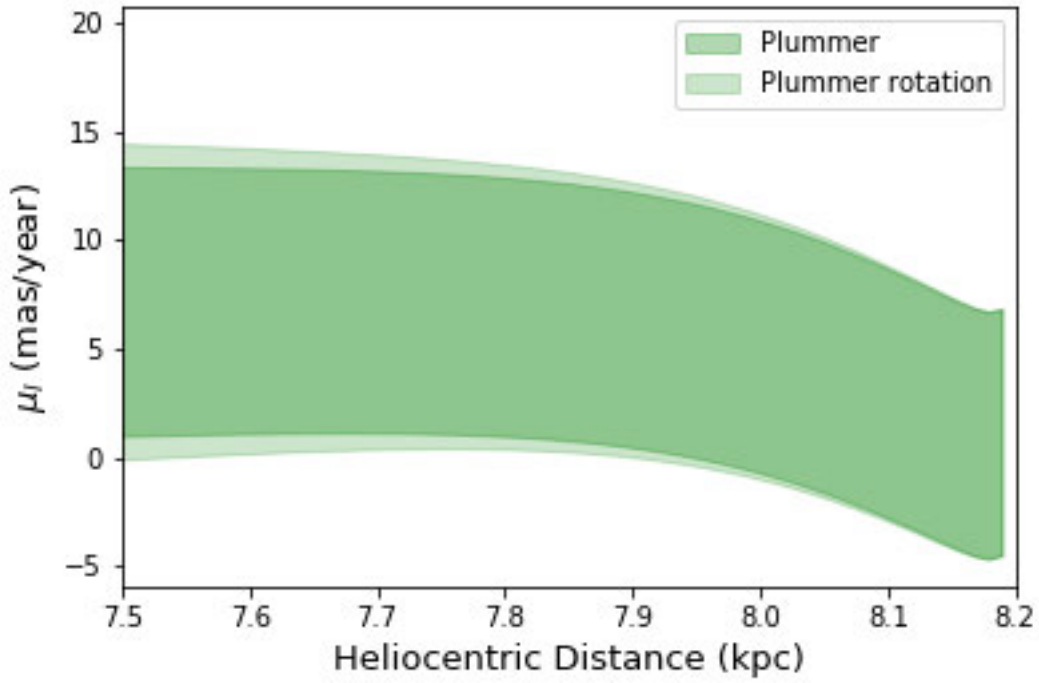

Figure 2-7: Proper motion distribution with additional pattern speed of $\Omega_b = 55km\ s^{-1}$. In this plot, the pattern speed of the bulge can result in the further broadening of the proper motion distribution of the nuclear bulge. At the heliocentric distance of 8.0 kpc, the discrepancy between two models is at approximately 0.3 mas/year.

rotating and non-rotating model.

Chapter 3

JASMINE Mission Parameters

3.1 History of JASMINE Mission

JASMINE (Japan Astrometry Satellite for Infrared Exploration) is the astrometric satellite mission selected by ISAS/JAXA to measure the positions and proper motions of celestial objects in the Galactic Nuclear Bulge region at about 100-300 pc from the Galactic Center. Initially, there were three main phases for the JASMINE mission, including nano-JASMINE, small-JASMINE, and medium-JASMINE.

3.1.1 Nano-JASMINE

Nano-JASMINE is a small astrometric satellite (size $50 \times 50 \times 50$ cm^3, weight 35 kg) designed to study and update the positions and proper motions of stars after 20 year-period of the Hipparcos mission. This mission is planned to be the second global astrometric mission and precursor mission for JASMINE. However, due to the delay in the launch site's construction, this mission became the third global astrometric mission after the launch of Gaia in 2013 [35]. The measurement of proper motion and parallax of Nano-JASMINE will be performed in scan-mode similarly to Gaia. The proper motion and parallax measurements of this satellite are performed on zw-band (0.6-10 μm) [12]. Besides, the precision of Nano-JASMINE in measuring the parallaxes and proper motions are $\leq$ 10 μarcsec and $\leq$ 4 μas/year respectively for

stars with a magnitude brighter than z = 14 magnitude [16].

From the 20-year baseline of this satellite, this mission is expected to update proper motion data up to 0.1 mas yr^{-1} and improved annual parallax accuracy to about 0.75 mas. With this new proper motion data, this satellite mission will resolve more binary star systems. Since Nano-JASMINE lacks photometry detectors, astrometric correction of target stars was performed using reference catalogs [35]. The combination of Nano-JASMINE with Hipparcos data will help astronomers to trace the structure of dark matter in the Milky Way [35]. Besides, combined data can help to distinguish long-period binary systems with a period from 6 to 40 years and determining their orbital elements [12].

3.1.2 Small-JASMINE

Small-JASMINE is the pioneer satellite of the JASMINE mission by JAXA. The small-JASMINE development plan was built upon the development of a catalog from the Gaia team and Nano-JASMINE software. This satellite mission will perform an astrometric measurement in Hw-band (1.1 μm - 1.7 μm) of the region near the Galactic Center to explore the formation and evolution history of the Milky Way. Small-JASMINE is expected to measure the parallaxes, and proper motions of about 67,000 bulge stars and about 31,000 disk stars for stars brighter than Hw $\approx$ 15 magnitude [34].

The expected launch date of Small JASMINE is around 2024, with a mission life of about three years. In 2020, the Small-JASMINE mission was renamed to JASMINE. This satellite is the satellite that we are focusing on in this study.

3.1.3 Medium-JASMINE

Medium-JASMINE was the mission intended to be launched in the late 2020s. The mission was planned to survey the region of $20^\circ \times 10^\circ$ square degrees around the Galactic Center. The satellite was proposed to have an aperture of 80 cm with a weight of 1500 kg. The observation would be performed in the Kw band (1.5 $\sim$

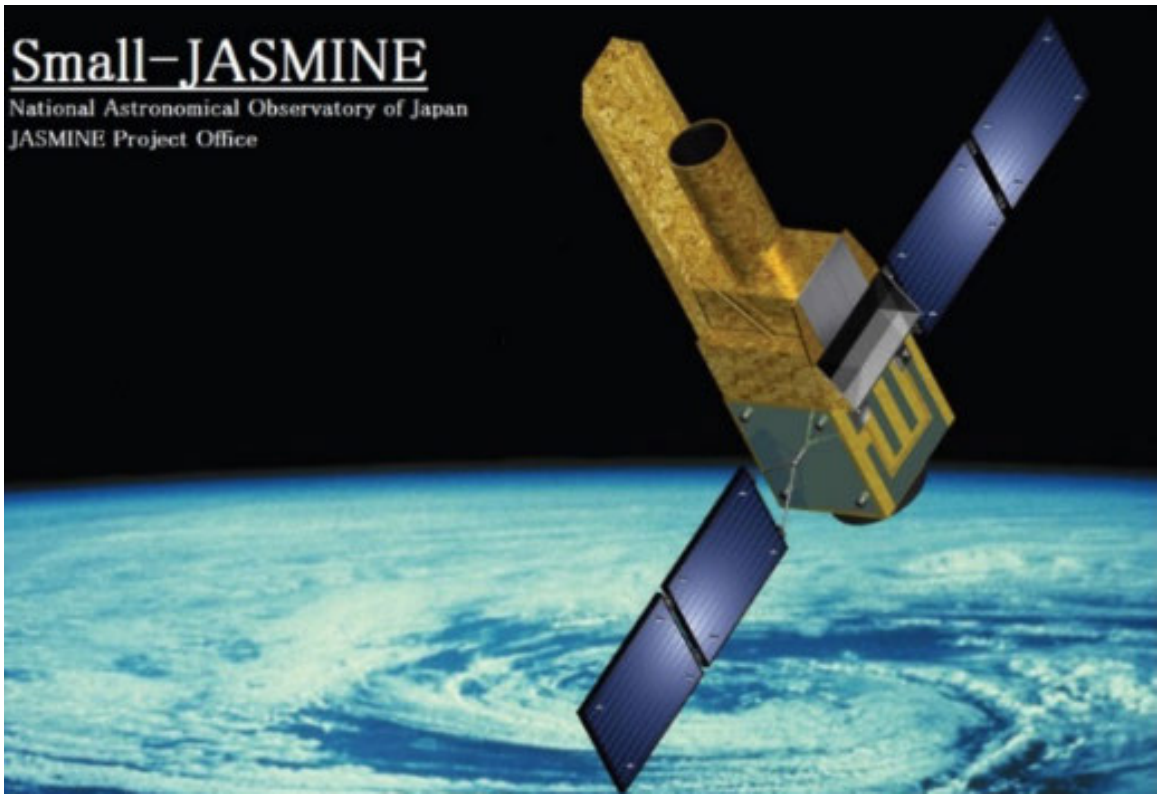

Figure 3-1: Concept art of Small-JASMINE satellite, taken from JASMINE mission description slides [34]

Table 3.1: The specification of the Bus module of JASMINE

Bus Size	1000 x 1000 x 1000 mm
Bus weight	200-250 kg
Mission Duration	3 years
Mission weight	$<$ 200 kg
Propulsion system	Reaction Control System (RCS)
Power	$<$ 300 W
Size	1000 x 1000 x size
Altitude control system	Three axis control
Altitude control Accuracy	$<$1 arcmin
Altitude control Stability	$<$ 0.1 mas/10 msec
Maneuvering	180 deg/10 min

2.5μm). The project aims to have the proper motion accuracy of 4$\mu as/year$ [11]. In the present day, the status of this project is uncertain.

3.2 JASMINE Satellite

JASMINE or former Small-JASMINE system consists of a bus module and mission module which compose of a telescope, electronics, sun shield, X-band antenna and GPS unit. The satellite is planned to be launched by Epsilon Launch Vehicle provided by JAXA. The orbit of the satellite is a sun-synchronized orbit at an altitude over 550 km. The specification of the JASMINE Bus module is described in Table 3.1 [34].

3.2.1 Telescope

The candidate of the optical system for the telescope is the modified Korsch system having three mirrors and four folding flats to fit the focal length into the available volume. The primary mirror has a 30 cm aperture size with a focal length of 3.9 m. CREARCERAM is selected as the candidate for materials of the telescope due to its low Coefficient of Thermal Expansion (CTE) at the operational temperature of the telescope (278 K) [34]. The field of view of the telescope is about 0.6×0.6 $degree^2$.

3.2.2 Orbits

JASMINE will be launched to the sun-synchronous Earth orbit by Epsilon launch Vehicle provided by JAXA [34]. This orbit has a period of approximately 90 minutes. The configuration of the telescope is to observe the Galactic Center during the time the telescope points in the opposite direction from the sun. One rotation of the satellite has the period of approximately half orbit or $\sim$ 45 minutes. With this orbit, JASMINE can observe the central region of the Milky Way only in spring and autumn. In summer and winter, JASMINE will observe other regions as the secondary objectives.

3.2.3 Survey Modes

JASMINE has two main survey modes depending on the time of the year. The key project of studying the Galactic Nuclear Bulge will be performed in spring and fall. In summer and winter, to prevent pointing the telescope toward the sun, JASMINE will study other interesting astrophysical objects. The potential missions during the summer and winter are exoplanet detection, bright objects in infrared bands, short-period astronomical phenomena, calibration for the data analysis [34].

The primary survey mode will be divided into two survey regions. Survey region 1 is the circle of radius 0.7 degrees around the Galactic Center. Survey region 2 is a rectangular survey region from galactic longitude -2.0 to 0.7 degree and galactic latitude from 0.0-0.3 degree as shown in Fig.3-2. The total solid angle of the two survey regions is approximately 1.9 square degrees or 6,900 square arcminutes.

The expected number of observable stars for survey region 1 is approximately 50,000 bulge stars and 26,000 disk stars for stars with magnitude $Hw < 15.0$. The expected number of observable stars for survey region 2 is roughly 29,000 bulge stars and 11,000 disk stars for stars with magnitude $Hw < 15.0$.

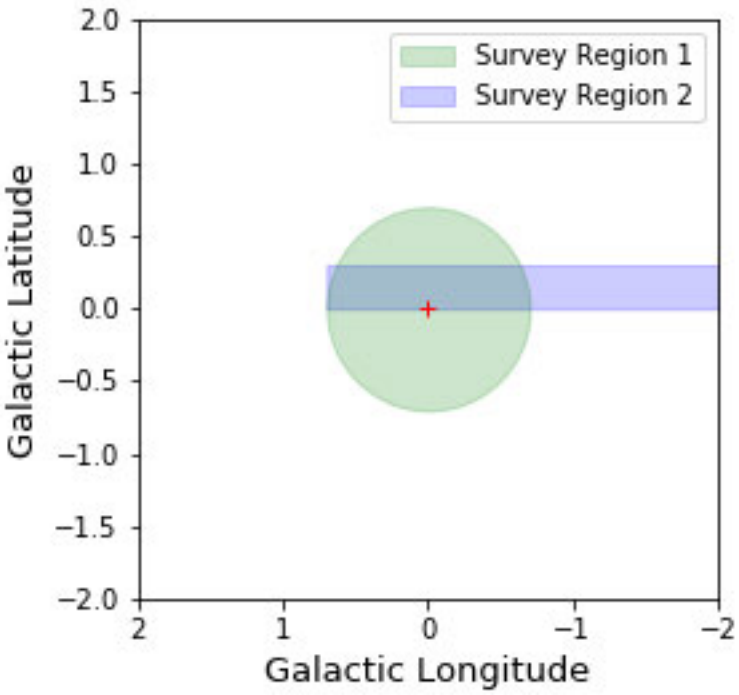

Figure 3-2: Survey regions for the key project of JASMINE in spring and autumn. Survey region 1 is a circle of radius 0.7 degrees around the Galactic center. Survey region 2 is a rectangle ranging from Galactic longitude -0.2 to 0.7 degree and Galactic latitude 0.0 to 0.3 degree.

3.2.4 Infrared Detector and Data Reduction

JASMINE operates in Hw-band at 1.1-1.7 μm. Hw-band can be approximated in terms of Johnson magnitude J and H as $0.7J + 0.3H$ [34]. The precision of angle measurement depends on the flux from the source. JASMINE has the precision of $<$25 μas for stars with Hw $<$ 12.5 mag, and $<$125 μas for stars with Hw $<$ 15.0 mag. During the mission, the infrared detector will be kept at the temperature of $T < 180K$. The detector has a pixel size of $10\mu m$ with the total number of 4096×4096 pixels. The value of read-out noise is 30e with the potential well of 100,000 [34].

Unlike its predecessors like Gaia or Hipparcos, JASMINE operates in near-infrared wavelength. This wavelength minimizes the interstellar extinction from galactic dust, revealing the structure of the central part of the Milky Way. In addition to the change in the passband, the data collection of JASMINE is also different from the previous astrometry missions. Hipparcos and Gaia gather data by scanning the detector across the field. On the other hand, JASMINE will observe the field in stare mode by taking images using a 2D detector. As a result, the data reduction and systematic of JASMINE will be different from its predecessors.

Observation of the survey regions will be performed by combining images with the size of Field of View together in the method called Frames-Link method. Each image will be taken in 7.1 seconds exposure and linked using various stars in the field that overlap region between adjacent fields. By combining the region of the same position for 20 frames, we can construct the small frames with the size of the Field of View of JASMINE. Then, the frame containing the entire observational region will be created by combining 16 small frames together to form a large frame. The approximate time to create a large frame is about 50 minutes which is equivalent to about half of the orbital period. Throughout three years of operations in autumn and spring, 8000 large frames of the observational area will be collected. By combining 8000 large frames, JASMINE will be able to determine the change of stellar positions to estimate parallax and proper motion of stars with correction of systematic error [34].

Table 3.2: The number of observable stars according to the mission specification.

Survey region	Bulge stars	Disk stars
Survey region 1 (Hw $<$ 12.5)	5,000	4,000
Survey region 1 (12.5 $<$ Hw $<$ 15.0)	45,000	21,000
Survey region 2 (Hw $<$ 12.5)	3,000	1,500
Survey region 2 (12.5 $<$ Hw $<$ 15.0)	26,000	9,500

With this specification, JASMINE is expected to measure about 67,000 bulge stars and 31,000 disk stars for Hw $<$ 15 mag. The approximate number of observable stars in each survey region according to the mission specification [34] is shown in Table 3.2

3.3 Scientific Objectives of JASMINE

Although JASMINE is designed to study the structure and evolution history of the Milky Way central core through high-precision measurements of proper motions and parallaxes, it can also be used in other missions as shown below [34].

1. Detection of exoplanets
2. To study the Hyper Velocity Stars (HVS) in the Galactic Nuclear Bulge
3. To study the origin of X-ray emission from X-ray binaries
4. To clarify the star formation rate in the nuclear bulge
5. Detection of unknown Black holes
6. To study the formation and motion of star clusters around the Galactic Center
7. Discovery of unknown objects

Chapter 4

Constraining Parameters of the Galactic Center Using JASMINE

In this chapter, we use the JASMINE specification mentioned in chapter 3 to evaluate the stars that JASMINE will be able to observe, the level of precision in the angle measurements, and the suitability of those stars for determining the kinematic structure of the bulge. Recall that JASMINE is expected to have parallax and proper motion precision of $< 25\ \mu as$ for stars with $Hw < 12.5$, and proper motion precision is expected to degrade as a function of signal-to-noise ratio to roughly $< 125\ \mu as$ at $Hw = 15.0$. Starting from these specifications, we aim to understand the precision JASMINE needs to study the structure of nuclear bulge and the size of the observable sample.

4.1 Parallax and Distance Distribution

The uncertainty in parallaxes measurement affects the distance measurement of stars in the bulge. Since we adopt the distance from the sun to the Galactic Center as 8.2 kpc [2] and approximate the radius of the Galactic Bulge as 2 kpc[34], we expect that the targets for JASMINE should stay within 10 kpc from the solar system. Since JASMINE aims to measure parallax with the precision of $< 25\ \mu as$, we can evaluate the goodness of this precision by studying the distribution and uncertainty of observed

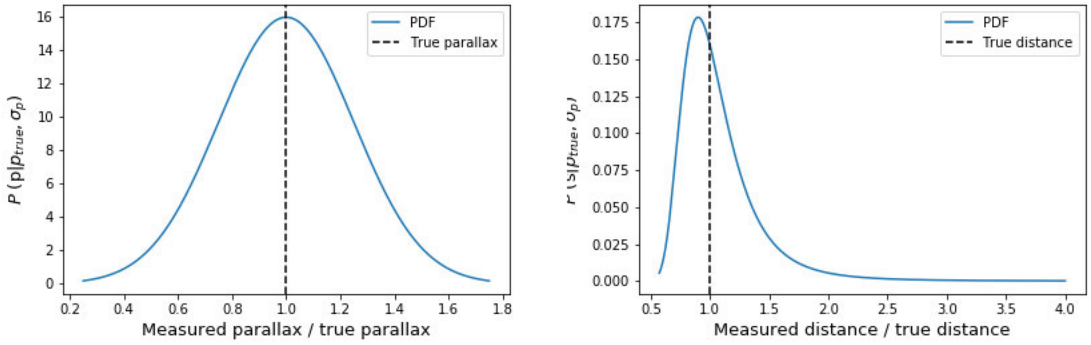

Figure 4-1: Plots showing the distribution of measured parallax and distance to stars at a distance 10 kpc from the sun with $\sigma_p = 25\ \mu as$. The left plot is the parallax distribution which is symmetric, while the right plot is distance distribution which the distribution is shifted to a lower value. This asymmetry is the result of the inverse relation between parallax and distance.

parallax and distance. In general, we expect the observed parallax to have Gaussian distribution, which can be written as

$$P(p|p_{true}, \sigma_p) = \frac{1}{\sqrt{2\pi}\sigma_p} \exp\left[-\frac{1}{2\sigma_p^2}(p - p_{true})^2\right] \tag{4.1}$$

However, since the true distance is inversely proportional to true parallax, this non-linear relation between parallax and distance deforms the observed distance distribution, making it asymmetric. [3] [18].

$$P(s|s_{true}, \sigma_p) = \frac{1}{\sqrt{2\pi}\sigma_p s^2} \exp\left[-\frac{1}{2\sigma_p^2}(\frac{1}{s} - \frac{1}{s_{true}})^2\right] \tag{4.2}$$

where s is the observed distance between observer and stars. The s^{-2} dependence in Eq.4.2 indicates that the distance distribution is asymmetric. Fig.4.1 shows the difference between the shape of the distribution of observed parallax and distance for stars at a distance 10 kpc from the observer.

From Fig.4.1, we notice that the peak of distance distribution is shifted to smaller values. This result indicates that the majority of the distance measured will be less than the true distance. Plotting various distance distributions with different parallax uncertainties σ_p shows that the shift becomes more significant as the uncertainties

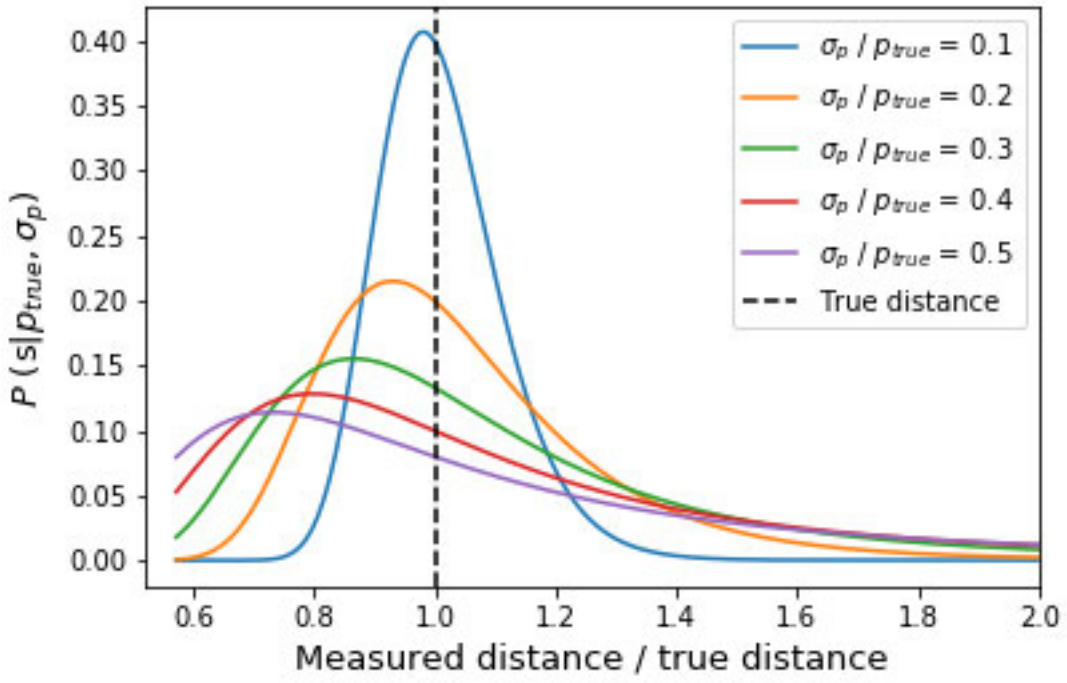

Figure 4-2: The plot of measured distance distribution compared to the true distance for different parallax uncertainties σ_p. This plot shows that distances are often underestimated for large parallax uncertainties.

grow. Therefore, we tend to underestimate the distance to targets from astrometric distance measurement, as shown in Fig.4-2.

This result implies that we need small enough parallax uncertainty to ensure that positions of stars are measured accurately. For example, if we approximate the radius of the nuclear bulge as the order of magnitude of 1 kpc, we need to ensure that a disk star locating at the distance of 10 kpc from the sun will not be mistaken as a part of the nuclear bulge. By plotting the position of the mode or the peak of distance distribution, we can indicate the reasonable precision that JASMINE needs to distinguish between disk stars and bulge stars as shown in Fig.4-3

Fig.4-3 shows that the mode of distance distribution has the value of approximately 90% of the true distance at parallax uncertainty of 25%. For stars at 10 kpc from the sun, this effect results in the measured distance of approximately 9 kpc which is approximately the boundary of Galactic Nuclear Bulge [34]. Since the true

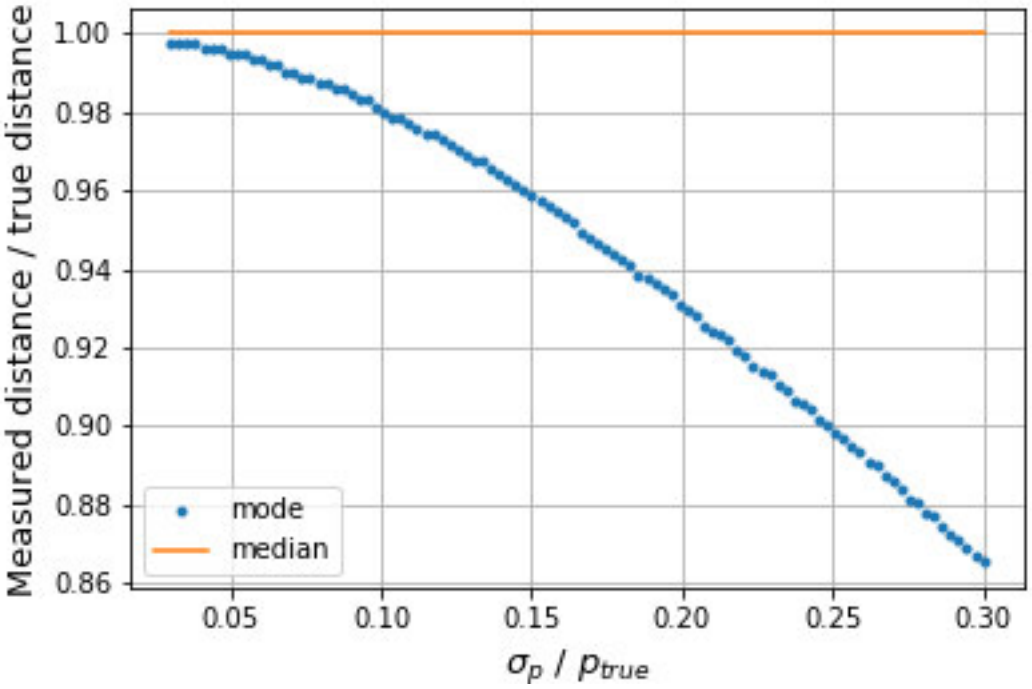

Figure 4-3: The plot indicating the position of the peak of measured distance distribution for stars locating at 10 kpc from the sun. This plot shows that the measured distance is decreasing as a function of parallax uncertainty.

parallax of a star at 10 kpc from the sun is 0.1 mas, the uncertainty of parallax measurement to distinguish between stars in nuclear bulge and disk star is 0.25×0.1 $mas = 25$ μas. Therefore, we conclude that it is reasonable for JASMINE to aim the parallax precision to be better than 25 μas.

In addition, from distance distribution, we can approximate the proportion of nuclear bulge stars that can be mistaken as stars in the outer bulge or galactic disk. Using the radius of the nuclear bulge as 1 kpc, we consider the distance distribution for stars locating at approximately the location of the Galactic Center. By performing numerical integration of the distribution function at the distance of ± 1 kpc from the Galactic Center, we can find the probability of stars near the Galactic Center to be measured to be in the nuclear bulge as shown in Fig 4-4. The result indicates that the probability for a star to be counted as the nuclear bulge star is 0.45. This result implies that about 45% of stars will be measured as a part of the nuclear bulge. Although the proportion is small, additional data about the population type of stars and kinematic properties of stars can help astronomers to distinguish between stars inside the nuclear bulge and stars in other part of the Milky Way.

4.2 Spectral Types of Stars Observable by JASMINE

JASMINE observes stars in Hw-band (1.1 μm - 1.7 μm; called H-wide). We can approximate the magnitude in this band using Hw $\approx$ 0.7J + 0.3H where J is the magnitude in J band, and H is the H band magnitude [34]. As we have discussed the importance of uncertainties of parallax and proper motion measurements, we can put the limit of parallax precision to be < 25 μas. The precision of parallax and proper motion measurements degrades with increasing magnitude. For instance, the stars that have magnitude Hw < 12.5 mag, JASMINE can measure the parallax to < 25 μas and proper motion < 25 $\mu as/yr$. For stars with Hw magnitude between 12.5 mag to 15.0 mag, the precision of proper motion decreases to about < 125 $\mu as/yr$. The difference of precision in stars with different brightness comes from the dependence of centroid precision on the signal-to-noise ratio which depends upon the detected flux

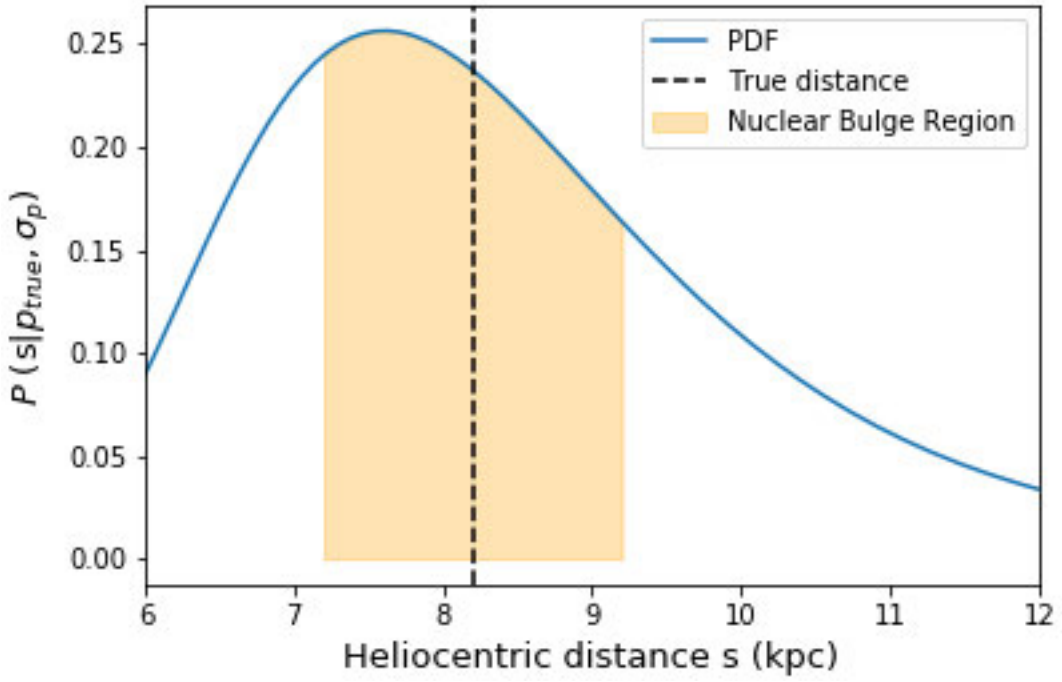

Figure 4-4: The plot indicating the probability of stars to be mapped as nuclear bulge stars for $\sigma_p = 25\ \mu as$.

of the source.

To find the spectral type of stars that can be observed by JASMINE, we can start by converting Hw band limiting magnitude of JASMINE to a more familiar band such as V-band. After converting Hw band magnitude into absolute V-band magnitude, we can use the Hertzsprung-Russell diagram or color-magnitude diagram to visually represent the proportion of stars that JASMINE can observe since Hw band magnitude can be approximated as the combination of J band and H band magnitude as the relation Hw $\approx 0.7\mathrm{J} + 0.3\mathrm{H}$ [34]. To simplify the calculation further, we assume that the Hw band magnitude can be represented purely by the J-band Johnson magnitude system.

Focusing at distance of 200 parsecs from the Galactic Center (8.0 kpc from the solar system), we convert J band limiting magnitude to absolute V band magnitude using

$$V = (V - J) + J + 5 - 5\log_{10}(d) - A_J \tag{4.3}$$

where $V - J$ is the color index of stars and A_J is the extinction coefficient ($A_J \approx 2.5$) [25].

Using the typical V magnitudes, B-V color indices, and V-J color indices from the Astronomy and Astrophysics handbook, we can speculate the spectral type of stars that can be observed by JASMINE as follows [37]

This Color-Magnitude diagram was plotted using lines indicating the spectral type of stars derived from Semiz & Ogur (2015) [33]. Each line is recreated in this thesis using the WebPlotDigitizer software [30]. Furthermore, the shaded part of the plot indicates the region of stars that can be observed by JASMINE. The color-magnitude diagram we created implies that the main targets for JASMINE are not main sequence stars, but are Giants and Supergiants. To describe the limiting absolute V-band magnitude for JASMINE to estimate the number of stars observable by JASMINE, we use the mean value of the limiting V-band magnitude across the color-magnitude diagram to represent the limiting absolute V-band magnitude of JASMINE. We find the mean value to be -3.20 at $Hw < 12.5$ and -0.70 at $Hw < 15.0$.

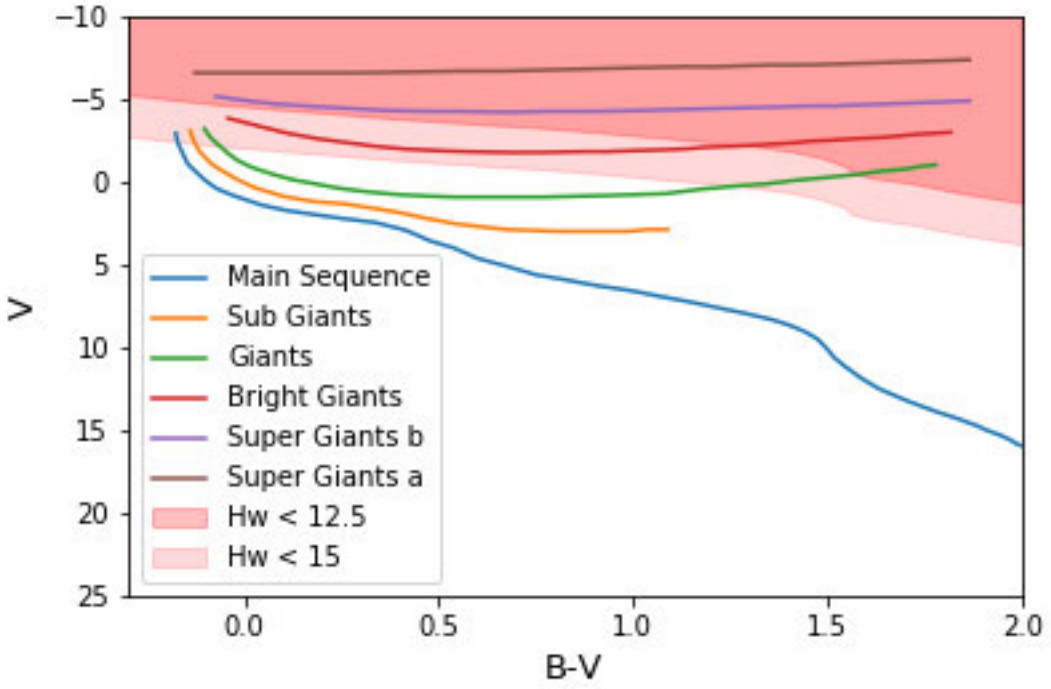

Figure 4-5: Color-Magnitude diagram showing the various spectral types of stars. The shaded region shows the stars that JASMINE can observe for J $<$ 12.5 and J $<$ 15.

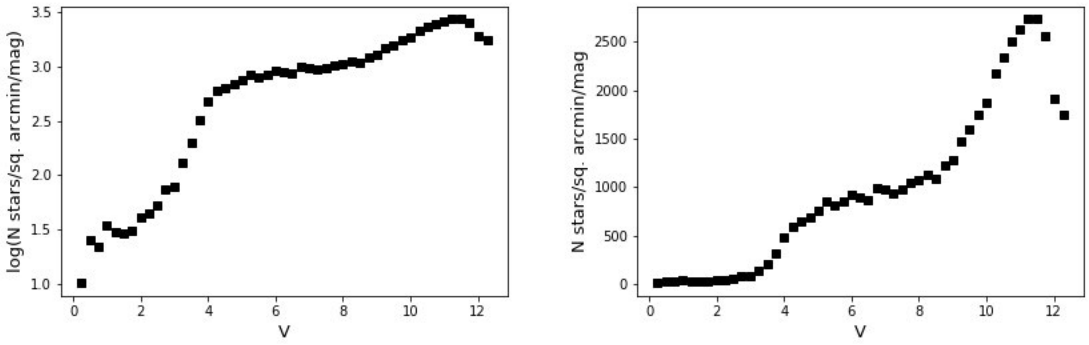

Figure 4-6: Luminosity Function as a function of absolute visual magnitude derived from the photometry of Baade's window [14]. The left plot shows the luminosity function in the log scale. The right plot shows the luminosity function in linear scale.

4.3 Number of Stars Observable by JASMINE

Another crucial part in designing the JASMINE mission is the sample size of observable stars. Using the limiting magnitude derived in the previous section, we can approximate the number of stars with the absolute visual magnitude less than the limit value using the stellar luminosity function.

In this thesis, we use the empirical Luminosity function of stars in V band derived from the photometry in the field of Baade's Window from Holtzman et al. (1998) [14] shown in Fig. 4-6. The Luminosity Function was extracted using WebPlotDigitizer software [30].

The number of stars with an absolute visual magnitude between V_1 and V_2 are derived from the integral of the luminosity function. Since the information on the number of stars that have a magnitude less than zero is not available in this plot, we have to extrapolate the plot to cover the range of magnitude that we are interested in. This can be done by fitting a function into the data and perform numerical integral on that function. One important requirement for the fit function to be physical is that this function has to converge to zero as V approaches $-\infty$. In this thesis, the candidate Luminosity functions that we consider as fit functions are Salpeter luminosity function and Schechter Luminosity function [7] [32].

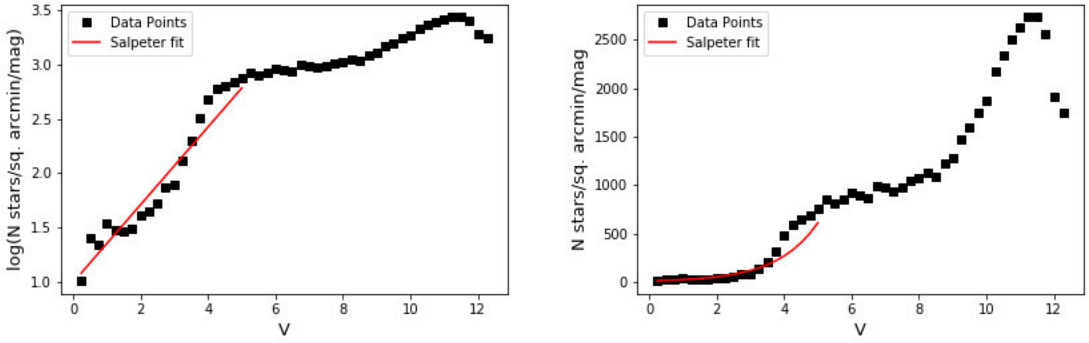

Figure 4-7: The plot showing the fitting of Luminosity Function using Salpeter Luminosity Function in log scale (left) and linear scale (right). The fit function fits well with the luminosity function at low absolute visual magnitude. However, the best fit deviates from the data points rapidly for $V > 4$

4.3.1 Salpeter Luminosity Function Fitting

Salpeter luminosity function is the luminosity function describing the proportion of Main Sequence stars in the absolute magnitude range $V = -4.5$ to $+13.5$ [31]. In Salpeter luminosity function, the shape of the luminosity function has the linear characteristic at the large luminosity. Therefore, we can write Salpeter Luminosity function as

$$log(\phi(L)) = c_1 V + c_2 \tag{4.4}$$

Eq. 4.4 is built based on the fact that the Salpeter Luminosity function has a linear form at high luminosity. We can try to fit a linear model in Eq. 4.4 to the data in Fig. 4-6. We try to create the linear fit for the luminosity function with $V < 4$.

From Fig. 4-7, the linear model does not fit well with the plot. We can evaluate the goodness of the fit using the chi-square χ value and chi-square per degree of freedom χ_{dof} defined in Eq.4.5 and Eq.4.6

$$\chi^2 = \sum_{i=1}^{N} \frac{(O_i - E_i)^2}{E_i} \tag{4.5}$$

$$\chi_{dof}{}^2 = \frac{\chi^2}{N-1} \tag{4.6}$$

where O_i is the value of each data point, E_i is the calculated value of luminosity function from the best fit, and N is the number of data points used in fitting, which is 16 data points.

From the plot in Fig.4-7, we notice that the linear fit diverges fast after V = 4. Thus, the shape of the fit function and the position of data points imply that this fit function is not a good fit. We can speculate further using the chi-square value. The chi-square value for the plot is $\chi^2 = 0.1903$ and chi-square per degree of freedom is ${\chi_{dof}}^2 = 0.0126$. We speculate that the discrepancy comes from the fact that the Salpeter Luminosity function is created to describe the Main Sequence stars. In addition, the Salpeter Luminosity function was created from the stars in solar neighborhood [31]. However, the main target for JASMINE are Giant stars in the Galactic Bulge. For this reason, there is a discrepancy in the fitting of this luminosity function.

4.3.2 Schechter Luminosity Function Fitting

Another candidate model for fitting the Luminosity function is Schechter Luminosity function which has the form

$$\phi(L)dL = \phi_\star \left(\frac{L}{L_\star}\right)^\alpha e^{\frac{-L}{L_\star}} \frac{dL}{L_\star} \tag{4.7}$$

where $L_\star$ and $\phi_\star$ are constants.

In general, Schechter Luminosity function describes the number of galaxies that have the luminosity between L and $L + dL$ [32]. Although Schechter Luminosity function is used for describing the number of galaxies for certain luminosity, it provides a simple model to describe the luminosity function at high luminosity and converges to zero for high luminosity stars. Therefore, Schechter Luminosity function is a good candidate for the fit as well.

Thus, we assume that the Luminosity function of stars has the same form as the Schechter Luminosity function. The region that we are interested in is the region with high luminosity or small absolute magnitude. Therefore, we consider fitting the

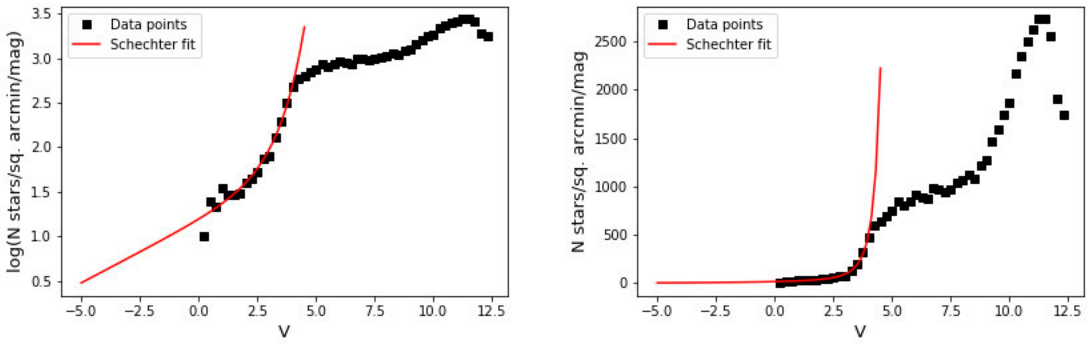

Figure 4-8: Luminosity Function fit using Schechter Luminosity function

function using data at the absolute visual magnitude of $V < 4$.

We can write Eq. 4.7 in terms of absolute visual magnitude V using the relation between Luminosity and visual magnitude

$$L_V = L_0 \cdot 10^{-0.4V} \tag{4.8}$$

where L_0 is the Luminosity of the star that has absolute visual magnitude of 0.

Plugging Eq.4.8 into Eq.4.7, we can rearrange the equation into the form

$$\log_{10}(\phi(V)) = -aV - b10^{-0.4V} + c \tag{4.9}$$

Fitting Eq.4.9 into Fig.4-6, we can find the best fit as shown in Fig.4-8

Similar to the Salpeter Luminosity function, we can evaluate the goodness of the fit using the chi-square value. From the calculation of chi-square value in Eq.4.5 and Eq.4.6. The result of the chi-square value calculation yields $\chi^2 = 0.0851$ and ${\chi_{dof}}^2 = 0.0057$. Since the χ^2 value of Schechter Luminosity function fit is less than that of Salpeter Luminosity function, we conclude that Schechter Luminosity function is a better fit function than Salpeter Luminosity function for the high luminosity part of the Luminosity function obtained from Holtzman et al. (1998) [14].

By having the fit function, we can extrapolate the luminosity function to cover the high luminosity part, we can then find the number of stars by performing integral

Table 4.1: The number of observable stars for JASMINE

Limiting Magnitude	Number of stars
$J < 12.5$	$1.2 \cdot 10^5$
$J < 15.0$	$2.6 \cdot 10^5$

of luminosity function as shown in Eq.4.10

$$N = \Omega \cdot \int_{-\infty}^{V_{limit}} \phi(V) dV \tag{4.10}$$

where V_{limit} is the limiting V band magnitude and Ω is the total solid angle of primary survey regions. In Chapter 3, we have shown that the area of survey regions is approximately 6900 square arcminutes.

The result of the number of stars that JASMINE expected to observe using Schechter luminosity function fit is shown in Table 4.1

Chapter 5

Discussions

5.1 Constraints to the Galactic Bulge

From our analysis in this thesis, we provide a simplified method to approximate the precision of JASMINE to distinguish different mass distributions, kinematics models, and the sample size for JASMINE observation.

5.1.1 Gravitational Potential constraints

In Chapter 2, we discuss the capabilities of JASMINE to distinguish the simplified models of the Galactic Nuclear Bulge by approaching from the kinematic viewpoint. By comparing limiting cases of compacting all masses at the center and homogeneous distribution of masses, we get a rough idea of the proper motion distribution of stars in the Galactic Bulge observed using JASMINE. The result indicates that the difference between the possible range of proper motion between two limiting cases at the distance of 200 pc from the Galactic Center is approximately 14 mas/year.

In addition, by studying the two kinematics limiting cases of pure bulk motion and pure pressure support system, the width of the distribution is significantly different between the two cases. For JASMINE to detect this difference, JASMINE needs to have proper motion precision better than 12 mas/year.

Therefore, JASMINE's proper motion precision of 125 μas/year or 0.125 mas/year

is more than enough to distinguish our limiting cases of mass distribution between point mass distribution and homogeneous sphere distribution, which require precision better than the order of 10 mas/year to distinguish.

5.1.2 Precision in Mapping Nuclear Bulge

In chapter 4, we show that another important factor to consider when we map the structure of nuclear bulge is the uncertainty of distance measurement. Although we can assume that the uncertainty of parallax measurement is normally distributed, the non-linear relation between parallax and distance makes the peak of distance distribution shift to smaller values compare to its median. This result implies that JASMINE tends to underestimate the distance to its targets. Our analysis shows that JASMINE needs the parallax precision of $< 25\ \mu as$ to avoid mistaken disk stars as nuclear bulge stars. Nevertheless, further analysis indicates that around 45% of stars with true distance within the nuclear bulge will be measured correctly as bulge stars. Hence, we also need additional data about kinematics and population type to distinguish these stars from disk stars or outer bulge stars.

5.1.3 Spectral Type Constraints

In Chapter 4, we approach the method of finding the Galactic Bulge constraints from the aspects of JASMINE specification. Since JASMINE is claimed to have the parallax precision of 125 μas for stars with $Hw < 15$ and precision of 25 μas for stars with $Hw < 12.5$, we can use the values of limiting magnitude to constrain the number of stars observable by JASMINE with high precision. By approximating JASMINE's Hw band as Johnson J band, the spectral types of stars that can be observed with high precision by JASMINE can be visualized using a color-magnitude diagram. Our result suggests that observable stars that can be mapped within 25 μas precision will be mainly main sequence O type stars and red supergiants. Moreover, for stars that can be mapped within the precision of 125 μas, the spectral type is extended to Giants. From this result, we can see that the primary targets for JASMINE are

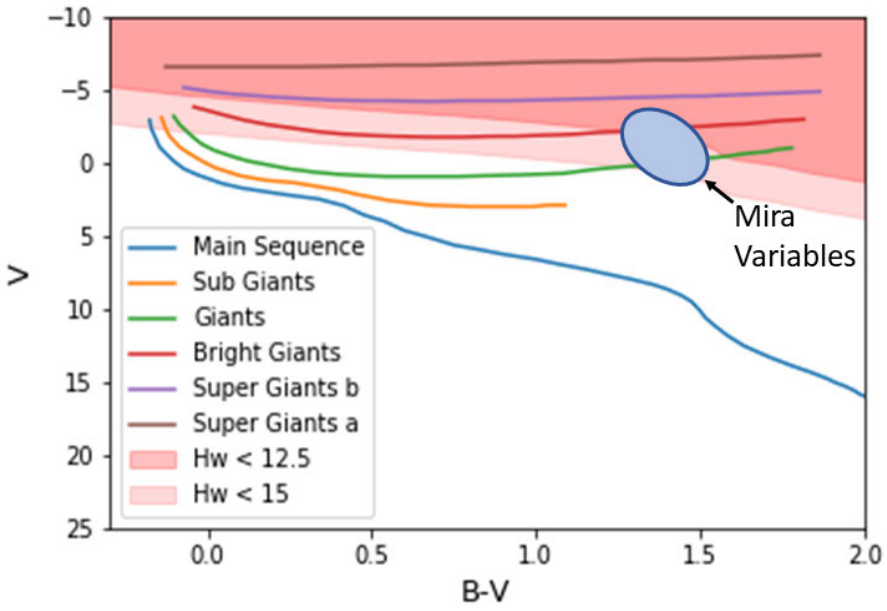

Figure 5-1: Color-Magnitude diagram showing the position of the instability strip of Mira variables, the main target of JASMINE. Mira variables reside within the observable part of the color-magnitude diagram, indicating that Mira variables are suitable targets for the JASMINE mission.

Giants and Supergiants.

As mentioned in JASMINE mission description [34], JASMINE will explore the structure of Galactic Nuclear Disk using Mira variables which are Long Period Variable (LPV) Stars. Since Mira variables are pulsating giant stars with bright and strong red color, Mira variables are good candidates for studying the Galactic Bulge structure using JASMINE. From our speculation with the position of Mira variables on instability strip on the color-magnitude diagram [36], the position of Mira variables on the color-magnitude diagram corresponds to the observable region of JASMINE discussed in Chapter 4 as shown in Fig.5-1. Therefore, JASMINE should be able to study the Galactic Bulge structure using Mira variables.

5.1.4 Sample Size

By using stellar luminosity function, we can approximate the total sample size of stars that can be observed by JASMINE. In this calculation, we compare two models of Lu-

minosity function: Salpeter Luminosity function and Schechter Luminosity function. From the chi-square values, we conclude that the Schechter Luminosity function is a better fit model for the high-luminosity end of the Luminosity function. The number of stars expected to be observed is approximately 260,000 for $J < 15.0$.

According to the JASMINE team [34], JASMINE claims to be able to observe 67000 bulge stars and 31000 disk stars which is 98000 stars in total for $J < 15.0$. The number of observable stars shown in Table 4.1 is about 2.7 times greater than the number of stars observable by JASMINE. Although the result is still in the same order of magnitude as the stars that JASMINE can observe, there are many possible causes for this discrepancy. For example, the calculation assumes that the Galactic Center has the same condition as the Baade's window. In fact, the interstellar extinction near the Galactic Center is higher than Baade's window. The interstellar extinction can reduce the number of observable stars significantly.

5.2 More Detailed Studies

In this thesis, there are various simplifications of the calculation. For example, in Chapter 2, we approximated that the total potential of the system is the combination of many potentials from various parts of the Milky Way. Especially at the Galactic Bulge region, we use a simplified model with spherical symmetry such as point mass model, homogeneous sphere, and Plummer model. In fact, the mass distribution near the center of the Milky Way has a strong X-shaped structure or boxy/peanut-shaped structure similarly to the central structure of other barred spiral galaxies [24]. The stellar mass in the X-shaped morphology accounts for approximately 7% of the mass of Galactic Bulge [28]. In our approximation, we neglect the effect of this structure and assume approximate the dynamics of stars as the collective potentials of the whole Galactic Bulge.

Besides, the presence of the Galactic Bar also introduces the non-axisymmetric gas flow and asymmetries in star counts. Nevertheless, in our approximation, we focus on the structure at radius 100 - 300 pc from the Galactic Center while the

galactic long bar can extend to about 5 kpc from the Galactic Center [28]. Using this approximation, we can reduce the effect of a larger structure outside the region of our modeling.

Another effect that we should discuss is the influence of dark matter in the Galactic Bulge. Dark matter can increase the radial force as a function of galactocentric radius up to approximately 50% of total radial force at the position of the solar system [29]. However, since we consider the system that stays at 100-300 pc from the Galactic Center, it is safe to consider this effect negligible.

One drawback of our calculation in this thesis is that the overall mass distribution model from Dauphole & Colin [7] that we use is the model for describing globular clusters around the Milky Way. As a result, this model might not be a perfect model to describe the dynamics of stars near the Galactic Center. Nevertheless, this model can provide a description of the external components that might affect the bulge, which is the primary region of interest.

In chapter 4, we also make several estimations to find the number of stars observable by JASMINE. For example, we approximate that the luminosity function of stars at the Galactic Center is the same as the luminosity function of stars at Baade's window obtained from Holtzman et al. (1998) [14] and fit the luminosity function using Schechter luminosity function. In general, the Schechter luminosity function is mainly used for finding the number of galaxies between two luminosity ranges. However, we use the Schechter luminosity function because it also fits well with the luminosity function we have. Our calculation also shows that the number of observable stars we calculated is also in approximately the same order of magnitude as the expected observable stars from the JASMINE mission specification. More information regarding the luminosity function near the Galactic Center is required to get a more precise calculation of the number of observable stars.

5.3 Conclusions

From our evaluation, we have shown that JASMINE has the capability to distinguish the gravitational potentials between two limiting cases: point mass and homogeneous sphere at the distance of approximately 200 pc from the Galactic Center. With the proper motion precision up to 125 μas/year or 0.125 mas/year, JASMINE should be able to distinguish the variation in proper motion in the order of magnitude of 10 mas/year at the distance of approximately 200 pc from the Galactic Center. Besides, JASMINE should be able to distinguish the rotating system from non-rotating system as well since JASMINE needs the precision of approximately 0.3 mas/year to resolve this.

Our analysis also yields the target sample of observable stars for JASMINE. The study of the observable section of color-magnitude diagram indicates that the primary targets for JASMINE are Giant and Supergiant stars. This result corresponds to the main targets of JASMINE, which are Mira variables. Hence, we can justify the use of Mira variables as the tracers for resolving the structure of the nuclear bulge. This analysis also leads to the approximation of the limiting absolute magnitude of stars that JASMINE can observe. Incorporating limiting magnitude with stellar luminosity function yields the number of observable stars of roughly 260,000 stars which are about 2.6 times greater than the number of stars claimed by JASMINE mission details.

Further studies are required to evaluate the capability of JASMINE further. Nevertheless, our studies give a rough approximation of JASMINE capabilities and confirm that JASMINE is a suitable satellite for probing the Galactic Bulge structure.

Appendix A

Upper and Lower Limits of Proper Motions in Different Gravitational Potentials

From our analysis in Chapter 2, we have created the upper and lower limit of the magnitude of proper motions of stars in the Galactic Bulge for the region around 500 pc from the Galactic Center in two limiting cases: pure bulk motion and pure random motion. The plots for individual models are shown in Fig.A-1 to Fig.A-3.

To understand the influence from other parts of the galaxy, it is useful to study the upper and lower limit at larger distance from the Galactic Center as well. In this

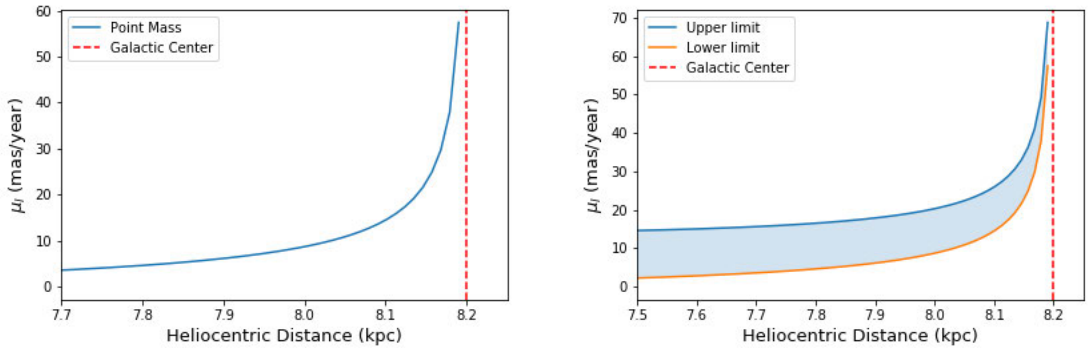

Figure A-1: Point mass model for heliocentric distance from 7.5 kpc to 8.2 kpc for pure bulk motion (left) and pure random motion (right).

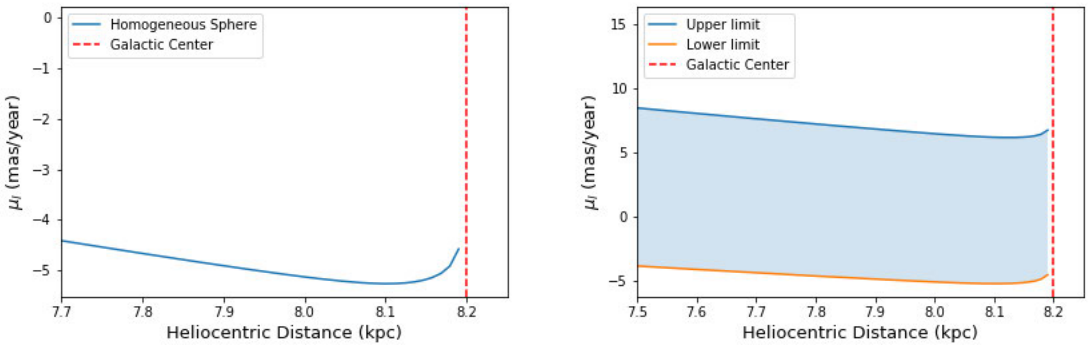

Figure A-2: Homogeneous Sphere model for heliocentric distance from 7.5 kpc to 8.2 kpc for pure bulk motion (left) and pure random motion (right).

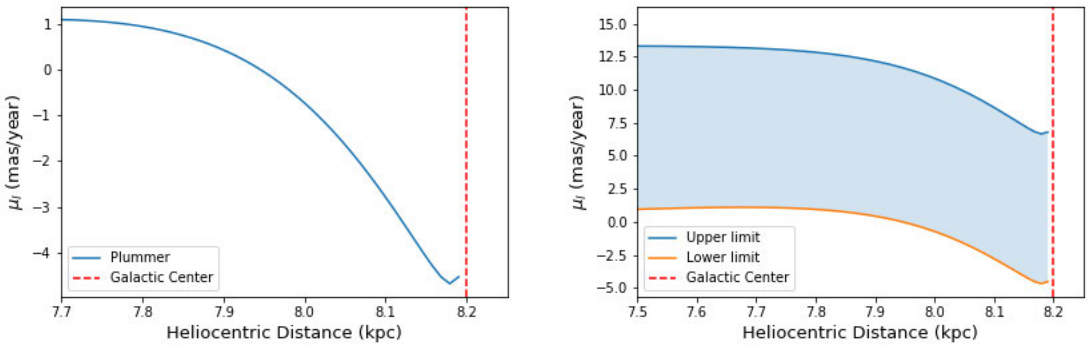

Figure A-3: Plummer model for heliocentric distance from 7.5 kpc to 8.2 kpc for pure bulk motion (left) and pure random motion (right).

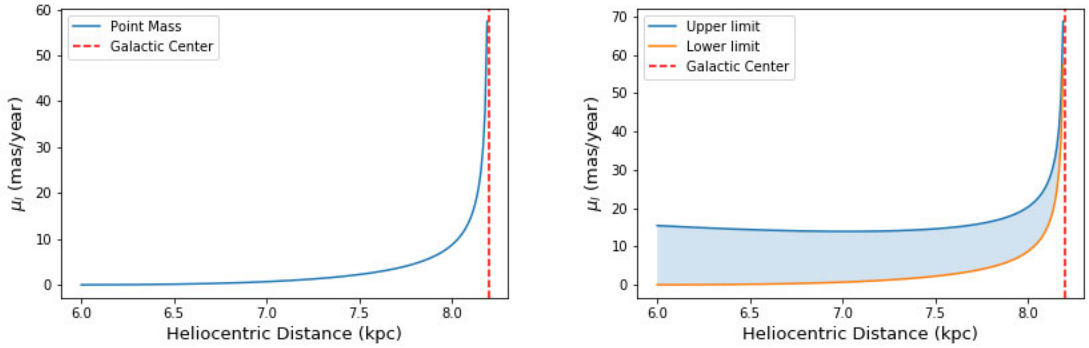

Figure A-4: Point mass model for heliocentric distance from 6.0 kpc to 8.2 kpc for pure bulk motion (left) and pure random motion (right).

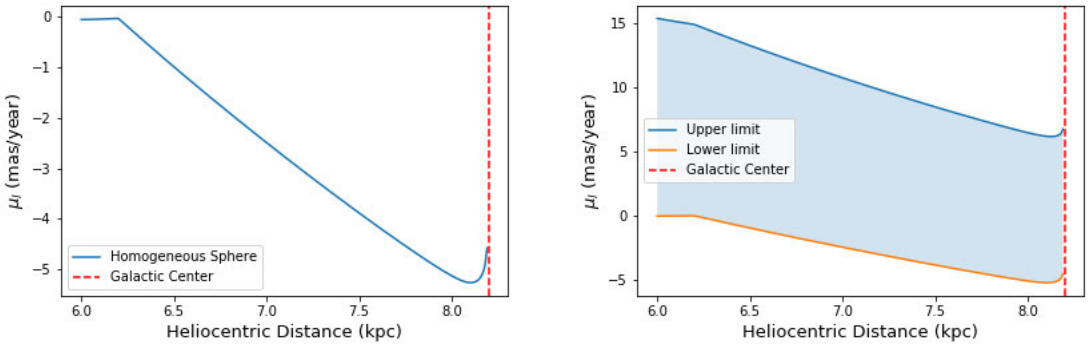

Figure A-5: Homogeneous Sphere model for heliocentric distance from 6.0 kpc to 8.2 kpc for pure bulk motion (left) and pure random motion (right).

case, we show the proper motion distribution from heliocentric distance 6 kpc to 8.2 kpc, or approximately 2 kpc around the Galactic Center in Fig.A-4 to Fig.A-7.

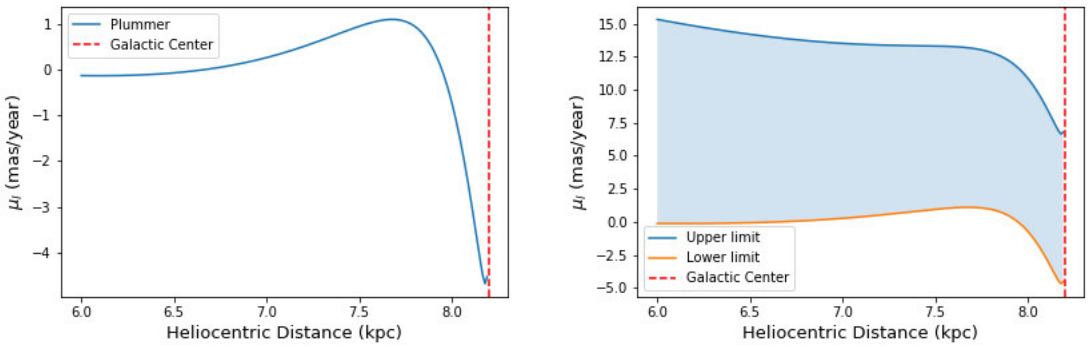

Figure A-6: Plummer model for heliocentric distance from 6.0 kpc to 8.2 kpc for pure bulk motion (left) and pure random motion (right).

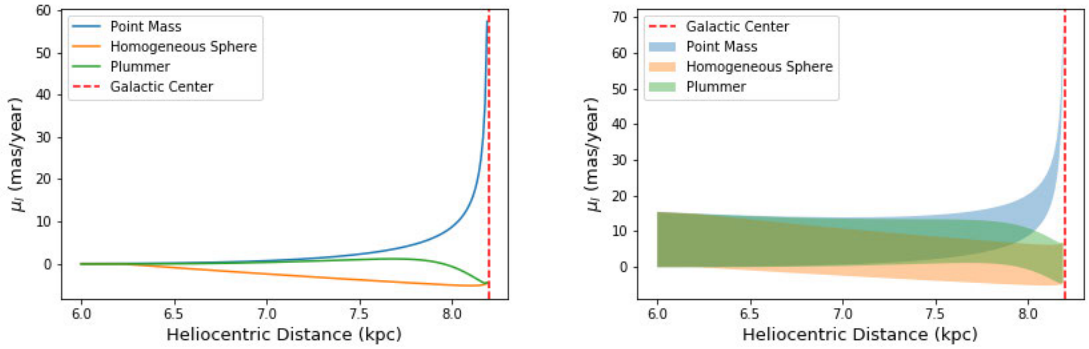

Figure A-7: Proper motion distribution for heliocentric distance from 6.0 kpc to 8.2 kpc for pure bulk motion (left) and pure random motion (right).

Bibliography

[1] *The HIPPARCOS and TYCHO catalogues. Astrometric and photometric star catalogues derived from the ESA HIPPARCOS Space Astrometry Mission*, volume 1200 of *ESA Special Publication*, January 1997.

[2] R. Abuter, A. Amorim, M. Bauböck, J. P. Berger, H. Bonnet, W. Brandner, Y. Clénet, V. Coudé du Foresto, P. T. de Zeeuw, and et al. A geometric distance measurement to the galactic center black hole with 0.3% uncertainty. *Astronomy & Astrophysics*, 625:L10, May 2019.

[3] Tri L. Astraatmadja and Coryn A. L. Bailer-Jones. Estimating distances from parallaxes. ii. performance of bayesian distance estimators on agaia-like catalogue. *The Astrophysical Journal*, 832(2):137, Nov 2016.

[4] James Binney and Scott Tremaine. *Galactic Dynamics: Second Edition*. 2008.

[5] John C. Brandt. St. Helena, Edmond Halley, the discovery of stellar proper motion, and the mystery of Aldebaran. *Journal of Astronomical History and Heritage*, 13(2):149–158, July 2010.

[6] Cristina Chiappini. The formation and evolution of the milky way. *American Scientist*, 89, 11 2001.

[7] B. Dauphole and J. Colin. Globular clusters as a new constraint for the potential of our Galaxy. *Astronomy & Astrophysics*, 300:117, August 1995.

[8] O. Gerhard. Pattern speeds in the Milky Way. *Memorie della Societa Astronomica Italiana Supplementi*, 18:185, January 2011.

[9] O. E. Gerhard. Structure and Mass Distribution of the Milky Way Bulge and Disk. In José G. Funes and Enrico Maria Corsini, editors, *Galaxy Disks and Disk Galaxies*, volume 230 of *Astronomical Society of the Pacific Conference Series*, pages 21–30, January 2001.

[10] A. Ghez, B. Klein, M. Morris, and E. Becklin. High proper motion stars in the vicinity of sgr a*: Evidence for a supermassive black hole at the center of our galaxy. *Astrophysical Journal*, 509, 07 1998.

[11] N. Gouda. Infrared Space Astrometry Missions ∼ JASMINE Missions ∼. In W. Aoki, M. Ishigaki, T. Suda, T. Tsujimoto, and N. Arimoto, editors, *Galactic Archaeology: Near-Field Cosmology and the Formation of the Milky Way*, volume 458 of *Astronomical Society of the Pacific Conference Series*, page 417, August 2012.

[12] Naoki Gouda. Small jasmine plan, Sep 2015.

[13] William Herschel. On the Construction of the Heavens. *Philosophical Transactions of the Royal Society of London Series I*, 75:213–266, January 1785.

[14] Jon A. Holtzman, Alan M. Watson, William A. Baum, Carl J. Grillmair, Edward J. Groth, Robert M. Light, Roger Lynds, and Jr. O'Neil, Earl J. The Luminosity Function and Initial Mass Function in the Galactic Bulge. *Astronomical Journal*, 115(5):1946–1957, May 1998.

[15] Mary Murray Hopkins. The Parallax of 61 Cygni. *Journal of the Royal Astronomical Society of Canada*, 10:498, November 1916.

[16] Herbert Kramer. Nano-jasmine.

[17] R. Launhardt, R. Zylka, and P. G. Mezger. The nuclear bulge of the galaxy. *Astronomy & Astrophysics*, 384(1):112–139, Mar 2002.

[18] X. Luri, A. G. A. Brown, L. M. Sarro, F. Arenou, C. A. L. Bailer-Jones, A. Castro-Ginard, J. de Bruijne, T. Prusti, C. Babusiaux, and H. E. Delgado. Gaia Data Release 2. Using Gaia parallaxes. *Astronomy & Astrophysics*, 616:A9, August 2018.

[19] David Merritt. *Dynamics and Evolution of Galactic Nuclei*. 2013.

[20] R. Miles. A light history of photometry: from Hipparchus to the Hubble Space Telescope. *Journal of the British Astronomical Association*, 117:172–186, August 2007.

[21] M. Miyamoto and R. Nagai. Three-dimensional models for the distribution of mass in galaxies. *Proceedings of the Astronomical Society of Japan*, 27:533–543, January 1975.

[22] David G. Monet. Introduction to CCD Astrometry. In Steve B. Howell, editor, *Astronomical CCD Observing and Reduction Techniques*, volume 23 of *Astronomical Society of the Pacific Conference Series*, page 221, January 1992.

[23] Paul Murdin. *Encyclopedia of astronomy and astrophysics*. 2001.

[24] Melissa Ness and Dustin Lang. The x-shaped bulge of the milky way revealed by wise. *The Astronomical Journal*, 152(1):14, Jun 2016.

[25] F. Nogueras-Lara, R. Schödel, F. Najarro, A. T. Gallego-Calvente, E. Gallego-Cano, B. Shahzamanian, and N. Neumayer. Variability of the near-infrared extinction curve towards the Galactic centre. *Astronomy & Astrophysics*, 630:L3, October 2019.

[26] Nogueras-Lara, F., Schödel, R., Gallego-Calvente, A. T., Dong, H., Gallego-Cano, E., Shahzamanian, B., Girard, J. H. V., Nishiyama, S., Najarro, F., and Neumayer, N. Galacticnucleus: A high-angular-resolution jhks imaging survey of the galactic centre - ii. first data release of the catalogue and the most detailed cmds of the gc. *Astronomy & Astrophysics*, 631:A20, 2019.

[27] H. C. Plummer. On the problem of distribution in globular star clusters. *Monthly Notices of the Royal Astronomical Society*, 71:460–470, March 1911.

[28] Matthieu Portail. Structure and dynamics of the galactic bulge and bar, October 2016.

[29] J I Read. The local dark matter density. *Journal of Physics G: Nuclear and Particle Physics*, 41(6):063101, May 2014.

[30] Ankit Rohatgi. Webplotdigitizer: Version 4.4, 2020.

[31] Edwin E. Salpeter. The Luminosity Function and Stellar Evolution. *Astrophysical Journal*, 121:161, January 1955.

[32] P. Schechter. An analytic expression for the luminosity function for galaxies. *Astrophysical Journal*, 203:297–306, January 1976.

[33] İbrahim Semiz and Salim Oğur. Dyson spheres around white dwarfs. *arXiv e-prints*, 03 2015.

[34] JASMINE team. Small-jasmine, May 2019.

[35] Yoshiyuki Yamada, Sho Fujita, Naoteru Gouda, Yukiyasu Kobayashi, Takuji Hara, Ryoichi Nishi, Satoshi Yoshioka, and Shunsuke Hozumi. Scientific goals of nano-jasmine. *Proceedings of the International Astronomical Union*, 8(S289):429–432, 2012.

[36] Donna Young. Pulsating variable stars and the hertzsprung-russell diagram. *The Earth Scienstist*, 28(1):20–26, 2012.

[37] Martin V. Zombeck. *HANDBOOK OF SPACE ASTRONOMY AND ASTROPHYSICS*. CAMBRIDGE UNIV. PR., 1984.